Micro-Images of Macro-Lensed Objects

by

Luke Weisenbach

Submitted to the Department of Physics
in partial fulfillment of the Requirements for the Degree of

BACHELOR OF SCIENCE

at the

MASSACHUSETTS INSTITUTE OF TECHNOLOGY

June 2018

Author .. Signature redacted .....
Department of Physics
May 11, 2018

Certified by... Signature redacted .....
Paul L. Schechter
William A. M. Burden Professor of Astrophysics, Emeritus
Thesis Supervisor

Accepted by Signature redacted .....
Professor Scott Hughes
Interim Physics Associate Head, Department of Physics

Micro-Images of Macro-Lensed Objects

by

Luke Weisenbach

Submitted to the Department of Physics
on May 11, 2018, in partial fulfillment of the
requirements for the Degree of
BACHELOR OF SCIENCE

Abstract

The study of gravitational micro-lensing at high optical depth has only rarely involved the close examination of the individual actual micro-images that arise as a result of the phenomenon. We discuss methods that refine on previous work done in the search for micro-images, which have been largely ignored in favor of other methods to study micro-lensing. With the help of magnification maps generated by Herr Prof. Dr. Joachim Wambsganss, we ran simulations that track positions and magnifications of micro-minima as functions of source position. We discuss the breakdown of a commonly used approximation for magnifications near fold caustics. Our results show that the approximation is noticeably broken at a caustic strength-scaled distance of 0.1. The relevance of this breakdown to work done by other authors is briefly examined. We then then discuss a few new results for the statistics of micro-images, deriving a formula for the mean micro-minimum magnification. We present a method for exactly calculating the caustic networks of micro-lensed systems, and calculate probability distributions for the caustic strength for two sets of parameters of interest. We present the creation of videos of the micro-lensing affect for pedagogical purposes. Finally, we briefly examine micro-lensing near macro-caustics and study the motion of micro-images as a point source crosses a macro-caustic.

Thesis Supervisor: Paul L. Schechter
Title: William A. M. Burden Professor of Astrophysics, Emeritus

Acknowledgments

First and foremost, I would like to thank Prof. Schechter for the amazing opportunities to learn that he has provided me with for the past two years. Without his help and guidance, I would not be where I am today.

I would like to thank my family back home, without whom I would not have reached MIT. Their continued love and support is the foundation upon which all else lies for me.

To Glen and Brad, thank you for your mentorship during highschool. I am fortunate to have been taught by you both, and to have formed such close friendships that have lasted beyond.

To Marcie and Matt, my many thanks for always welcoming me into your home when I visit. I am always humbled by your patience and kindness.

To Michael, Luke, Sean, Brandon, and Josh - my life would not be the same if I had not met you all. May the coming years prove as wonderful as the past have been.

To James and Abby, thank you for always being there whenever I need you most. You both exemplify every good aspect of what I strive to be as a person.

Lastly, many thanks to my friends at MIT. To all those in A Entry who gave me my second home for three years, you have my deepest thanks. To the brothers of ΣAE, I cannot state how much I cherish the time I have spent with y'all. I would not have grown into to the person I am today without you.

Contents

List of Figures

List of Tables

Chapter 1

Introduction

1.1 Gravitational lensing

When you look out at the stars at night, even when it is as clear as can be, there is a distinct twinkling that fails to ever really go away. This is in large part due to the Earth's atmosphere causing minuscule fluctuations that disturb the waves of light your eye receives.

The phenomenon of intervening matter disturbing the light from a distant source is not limited to light passing through the atmosphere. On a larger scale, light from a very distant background source that passes through an intermediate galaxy on its way to us also appears to twinkle and fluctuate over time. Even more remarkably, there can sometimes appear multiple images of the same object in the sky. Confirmation comes through both spectral analysis and the presence of general large scale features over time that appear in the lightcurves of all the images (albeit shifted in time).

Einstein's theory of relativity provides the explanation for this. In essence, the presence of an intervening mass distribution (in this case, a galaxy) between an observer and a properly aligned background source acts as a lens, magnifying the light received from the source. In addition, the curvature of spacetime by massive objects can provide multiple geodesics for light to reach us, as Fermat's principle states that light travels along paths which are local stationary points of the travel time.

Gravitational lensing provides a way to study objects located behind a galaxy

which we may otherwise be unable to see, and lends itself to studying not only the makeup of the lensing galaxy but also the source itself as well through the variations in the light we receive.

The most interesting features in the lightcurve of a source are periods of highly increased magnification, which typically occur during events known as caustic crossings. During such events, the number of images increases or decreases by two, leading to a large change in flux received.[1] There exist approximations for the temporal variations in flux of an ideal point source near such an event, but these approximations are known to break down outside a certain regime. Additionally, parameters that characterize the approximation cannot be observed. In general, these events can only be analyzed statistically for micro-lensing with current observational abilities.

For an extended source, the observed temporal variation is the convolution of the source profile with the temporal variation of a point source. A better understanding of the behavior of point sources near caustic crossings will help in the analysis of extended sources, as the high magnifications near caustic crossings are easier to observe and thus are most valuable for learning about source profiles.

We therefore set out with the main goal of examining the behavior of micro-images near caustic crossing events. From there we will branch out slightly to other areas which either aid or supplement our analysis and understanding of micro-images, as well as extend our methods to further regions of interest.

1.2 Outline for the thesis

In Chapter 2, we provide a background to lensing and present the relevant mathematics needed while building up some important concepts.

In Chapter 3, we discuss the development and refinement of methods to search for the locations of all the micro-images of a point source produced by a random star field. The behavior of micro-images near caustic crossings is examined, with an analysis

[1] For the majority of our study, this means the number of *micro-images* changes by two. However, Chapter 7 will briefly discuss when the number of *macro-images* changes by two and how the number of micro-images is affected as well.

of the approximations commonly used. The breakdown of such approximations is discussed, along with how the regime wherein the breakdown happens affects analyses of previous work.

In Chapter 4, we discuss some statistical results for mean micro-minima magnifications using extensions of previous work. We raise the question of the possibility of deriving probability densities for caustic strengths. We provide the steps necessary for such a derivation, which relies upon an integral that we were unable to easily evaluate, approximate, or simplify.

In Chapter 5 we present a method to calculate the caustic network of a field of stars. We perform simulations and determine the probability distributions for caustic strengths for two sets of parameters of interest.

In Chapter 6 we discuss the animation of the creation and annihilation of pairs of micro-images, and the creation of a video for pedagogical purposes.

In Chapter 7, we briefly begin to look at how our work can be extended to the regions around macro-caustics. We examine the motion of micro-images as a point source crosses the micro-caustic network of a macro-caustic.

In Chapter 8, we provide a brief summary of our work and some ending remarks.

Chapter 2

Basics of Gravitational Lensing

2.1 A difference in scale

2.1.1 Macro-lensing

On a macro-scale, a galaxy as a whole (or a cluster of galaxies) provides a smoothed out matter distribution that acts as a lens, with an effective index of refraction that can vary in locations throughout the galaxy depending on how the matter is distributed. These variations produce the multiple macro-images of a background source that are spatially resolved in the sky. The light received from these images fluctuates over cosmic time scales due to movement between the source, lens, and observer. Fluctuations visible in all the macro-images must be due to intrinsic source variability. However, additional small scale fluctuations appear which differ from macro-image to macro-image that are not explainable as such.

2.1.2 Micro-lensing

The matter in a galaxy is in actuality not all smoothly distributed. In addition to dark matter (which is assumed to be a smoothly varying component with particles of $mc^2 \approx 1GeV$), the baryonic matter in a galaxy is discretely packeted into components such as stars and planets. These components act as micro-lenses in their own right, creating thousands of unresolvable micro-images that together make up the macro-

image. The movement and changes in the flux from these micro-images in total produces the flux variations we can actually observe in the macro-images.

Due to the fact that these micro-images are not directly observable, their properties must be studied through simulations, in order to be able to statistically analyze observed events.

2.2 Relevant equations and variables

The grittier details of lensing have been explored elsewhere, e.g. [2], [10], and [12]. We will take as given the following facts in examining the local affects of micro-lensing at the location of one particular macro-image.

1. The function $\tau(\vec{x}) \propto \frac{1}{2}(\vec{x} - \vec{y})^2 - \phi(\vec{x})$ gives the time delay at a point $\vec{x}$ in the image plane for light from a source at position $\vec{y}$ in the source plane. This delay is due to a geometrical offset, and the Shapiro time delay due to the gravitational potential ϕ caused by a mass distribution in the image plane. The coordinate systems for $\vec{x}$ and $\vec{y}$ are taken to be concentric, and with similarly oriented axes. τ here is taken to be dimensionless, as the proportionality factor depends only on physical constants and distances between source, lens, and observer. The size of the intervening mass distribution is taken to be much less than the distances between source, lens, and observer, so that the thin lens approximation can used. ϕ is then an integral of the three dimensional gravitational potential along the line of sight.

2. Fermat's principle tells us that images are located at positions $\vec{x}$ which are local stationary points of the travel time, i.e. where $\nabla_{\vec{x}}[\tau(\vec{x})] = 0$. Note that for no intervening mass distributions, this gives $\vec{x} = \vec{y}$, as expected - we only see one image located precisely at the position of the source, as any deviation would only increase the light travel time.

3. 1 and 2 together give the lens equation, $\vec{y} = \vec{x} - \nabla_{\vec{x}}[\phi(\vec{x})]$.

4. The lens equation in the vicinity of a macro-image can be taken to have the form

$$\vec{y} = \begin{pmatrix} 1-\kappa-\gamma & 0 \\ 0 & 1-\kappa+\gamma \end{pmatrix} \vec{x}.$$

The convergence $\kappa \propto \nabla^2\phi$ is (through Poisson's equation in two dimensions) a dimensionless surface mass density in the area of interest. The shear $\gamma > 0$ is a tidal distortion due to the global presence of the rest of the galaxy that has a constant value locally. Depending on the values of κ and γ, small changes in source position can induce large changes in image location. However, equal variations in source location Δy will produce equal deflections Δx.

5. The coordinate system has been oriented such that the inverse magnification matrix

$$A = \frac{\partial \vec{y}}{\partial \vec{x}} = \begin{pmatrix} 1-\kappa-\gamma & 0 \\ 0 & 1-\kappa+\gamma \end{pmatrix}$$

is diagonal (which is always possible to achieve). This dictates two principal directions, along which the image of a circular source will be stretched or compressed to produce an ellipse.[1] The magnification μ of an image is a ratio of the size of the image to the size of the source, and is equal to $\mu = \frac{1}{\det A}$. For the macro-image, the mean magnification is

$$\langle \mu_{macro} \rangle = \frac{1}{(1-\kappa)^2 - \gamma^2}.$$

Magnifications may be positive or negative, depending on the signs of the eigenvalues of A (or equivalently the shape of τ at the location of an image). A saddle point of τ corresponds to a negative magnification, which is interpreted as a parity flip of the image. A minimum or maximum of τ will be of positive magnification.

6. The presence of micro-lenses, such as stars, in a matter distribution breaks the

[1] It is the shear which causes such an effect. Convergence alone only alters the size, and so equivalently the magnification, of the image of a source.

smoothness of the gravitational potential on some scale. For micro-lensing, the lens equation can be taken to have the form

$$\vec{y} = \begin{pmatrix} 1 - \kappa_{dark} - \gamma & 0 \\ 0 & 1 - \kappa_{dark} + \gamma \end{pmatrix} \vec{x} - \theta_E^2 \sum_{i=1}^{N} \frac{m_i \cdot (\vec{x} - \vec{x_i})}{|\vec{x} - \vec{x_i}|^2},$$

where κ_{dark} is now the surface mass density in smoothly distributed dark matter, and γ is unchanged. The stars are taken to be point masses located at the $\vec{x_i}$ in the source plane, and the m_i are the masses of the stars in terms of a unit mass. This unit mass determines θ_E, a distance scale known as the Einstein radius which depends on the unit mass used, physical constants, and distances between source, lens, and observer. The covering factor of the stars, $\kappa_\star = n \sum_{i=1}^{N} \pi \cdot \theta_E^2 \cdot m_i$ where n is the number density of stars, provides an effective convergence. Together, $\kappa_\star + \kappa_{dark}$ provide the total κ present in the lensing equation for a macro-image.

7. For a given source position $\vec{y}$, there are now multiple image positions $\vec{x}$ which solve the lens equation, thus producing the multiple micro-images. The magnification μ of an individual micro-image is again still equal to $\frac{1}{\det A}$, where $A = \frac{\partial \vec{y}}{\partial \vec{x}}$ is evaluated at the image location. However, as our coordinate system is oriented along the principal axes of the global shear, A is no longer necessarily diagonal at the location of each micro-image. The individual stars provide their own shear which does not necessarily align with the global shear, thus producing off-diagonal terms in A (though of course A can still be diagonalized at the yet more local position of a particular micro-image, producing a coordinate system where the global shear would have off-diagonal terms).

For our analysis, we will assume that all masses are equal to $1 M_\odot$ and use θ_E as our unit distance (in the image plane, and an appropriately source-image-distance scaled θ_E in the source plane). In addition, Paczynski has shown that the presence of κ_{dark} simply amounts to a scaling of γ, $\kappa_\star$, and μ [12]. Thus we can set $\kappa_{dark} = 0$ without loss of generality.

2.3 Building up a macro-image from micro-images

Examining the lens equation without any perturbing stars for a moment, we see that there is a unique image location for every source position, whose position is simply scaled from the source position by factors involving γ. The time delay for sample configurations are shown in figure 2-1, corresponding to a macro-saddlepoint and a macro-minimum.

Adding a single star to the smoothed out matter distribution perturbs the smoothed out time delay function and adds additional solutions to the lens equation. This typically results in an additional saddle point close to the star, as can be seen in the zoomed regions in figure 2-1. Continuing the procedure with stars appropriately far away from the location of the macro-image produces many micro-images (namely saddle points) which are "associated" with a star in the field. As one adds more stars, particularly close together and near to the original location of the macro-image, depending on the configuration of stars there may appear micro-minima in addition to micro-saddles.

2.4 Critical curves and caustics

The inverse magnification matrix $A = \frac{\partial \vec{y}}{\partial \vec{x}}$ varies smoothly as a function of $\vec{x}$ over the image plane. The locus of points where $\det A = 0$ form what are known as the critical curves. The mapping of this set to the source plane forms a locus of points known as the caustics. Caustics form the boundaries between regions with varying numbers of micro-images.

The case of a single perturbing star in a field with external shear has been extensively studied already, starting with Chang and Refsdal in [3] and [4], and more recently by An and Evans [1], and is known as the Chang-Refsdal lens. The critical curves and caustics for such a system corresponding to a macro-saddle (taken to be similar, but slightly different than that of figure 2-1) are shown in figure 2-2.[2] For a source located outside the caustics, there are two micro-images: that corresponding

[2] A macro-saddle requires a shear $\gamma > 1$, and a minimum requires $\gamma < 1$.

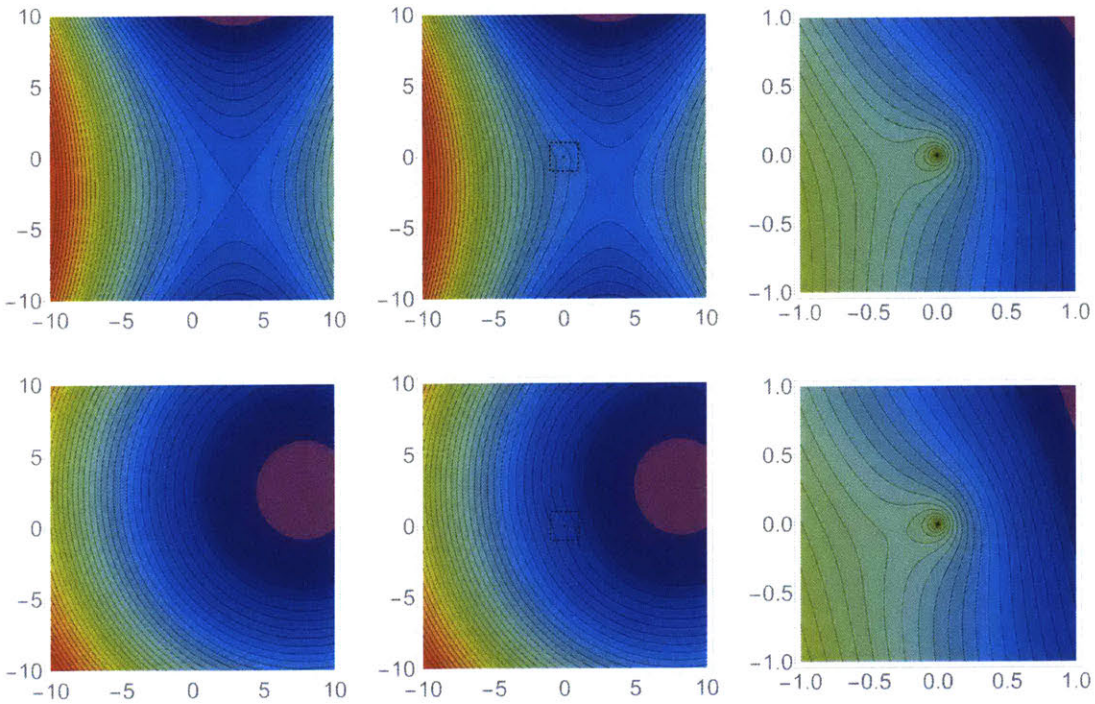

Figure 2-1: Sample time delays for a macro-saddle and a macro-minimum
Top: Sample time delays of a macro-saddle. From left to right: time delay of the smoothed-out matter distribution, time delay with the presence of one perturbing star, zoom of the boxed area. Bottom: Sample time delays of a macro-minimum. From left to right: time delay of the smoothed-out matter distribution, time delay with the presence of one perturbing star, zoom of the boxed area. In both cases the position of the source is taken to be (3,1) in the source plane, which is concentric with the image plane and aligned with the same axes. The location of the macro-image has been ever-so-slightly perturbed after the addition of the star in both cases. Note that the introduction of a star technically adds another root (a micro-maximum) to the lens equation in addition to the saddle point, which can be found at precisely the location of the star. However, the travel time there is formally infinite and the image is infinitely de-magnified.

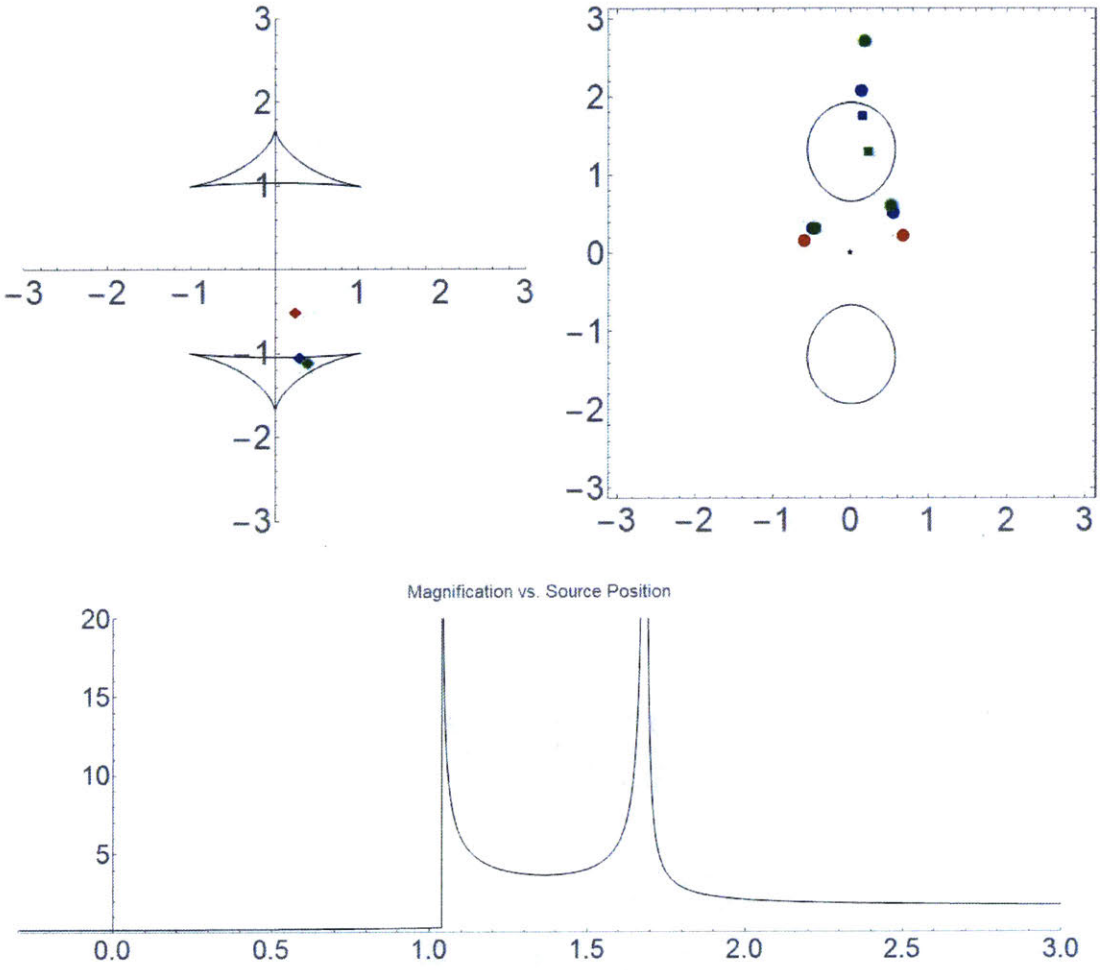

Figure 2-2: Sample lightcurve for a Chang-Refsdal Lens
Counterclockwise from top right: Critical curves in the image plane for a star at the origin, caustics in the source plane, and magnification as a function of source y-position for a source moving along a track in a straight line from (0,-0.3) to (0,3). The system examined here is one with external shear corresponding to a macro-saddle. The colored squares and circles in the image plane correspond to the micro-minima and micro-saddles (respectively) of like colored sources. Note the formation of an extra pair of images for the blue source which has just crossed a caustic.

to the original unperturbed image of the source, and the associated saddle point for the perturbing star. As a source moves inside one of the diamond shaped caustics, a pair of micro-images is created somewhere along the critical curves. The pair of images which are created (or annihilated) always consists of a micro-minimum and a micro-saddle. At their point of creation, each micro-image has formally infinite magnification (as $\det A = 0$ on the critical curve) that quickly decreases as the source moves away from the caustic. The lightcurve for a source moving along a track up the y-axis is shown as well in figure 2-2, and the net magnification as a function of source position is shown in figure 3-1.

For many stars that are far apart, the caustics are separated. However, increasing $\kappa_\star$ "grows" the caustics into a network such as that seen in figure 3-1. A visualization of the process can be found in figure 2 of [14] with appropriate discussion.[3]

[3]There are a couple of ways to think of this "growing", both of which are valuable in their own right. The macro-saddle is first created by an appropriate combination of γ and $\kappa = \kappa_{dark}$. Adding one star in the ideally infinite area contributes no $\kappa_\star$, as the number density is zero. But, as more stars of equal mass are added and the number density increases, one can take away from κ_{dark} such that the sum $\kappa_\star + \kappa_{dark}$ stays constant (thus keeping the mean macro-magnification that of a saddle). The addition of each star produces new micro-images, as well as new caustics which stack on top of each other. Thus, a source at a particular position may go from having 0 micro-minima to multiple micro-minima if the caustics stack up enough. Alternatively, one could keep the number density of the stars constant from the start (with infinitesimally small mass), and slowly increase their mass until the appropriate $\kappa_\star$ desired is reached. This would produce many thousands of caustics centered on the positions of the stars that slowly grow into a network as mentioned.

Chapter 3

Caustic Crossings and Behavior of Micro-Images

3.1 Magnification maps

One of the most common computational methods of studying gravitational microlensing is through the use of magnification maps. These maps provide net source magnification as a function of position in the source plane for various parameters. There are two commonly used methods for creating such maps.

One method, the inverse ray shooting method (IRS), traces rays of light backwards through a large field of stars from the image plane to the source plane, collecting the rays in pixels and assigning a magnification proportional to the number of rays that land on each pixel. Another method, inverse polygon mapping (IPM), calculates the distortion of shapes through the mapping of the lens equation from image to source plane, assigning magnifications based on area ratios [9].

Both methods provide information on the total magnification as a function of source position, as well as visualizations of the caustic networks as in figure 3-1. However, neither provides information as to how individual micro-images and their various properties change. In order to do so, one must locate each individual micro-image produced for a given source position, and track their positions, magnifications, and other properties of interest as the source moves.

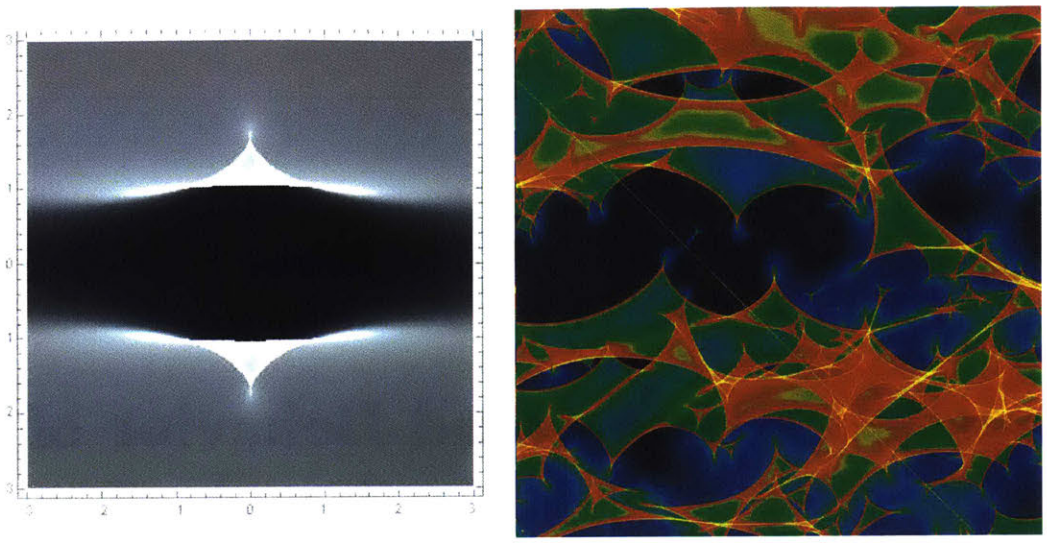

Figure 3-1: Sample magnification patterns
Left: Total magnification as a function of source position for the Chang-Refsdal lens shown in 2-2. Total magnification is grey-scaled, with black corresponding to de-magnification from average and white corresponding to higher magnification than average. Note the sharp borders (which line up with the locations of the caustics), and areas of high magnification around (yet outside) the cusps. A source located directly behind the position of the star is highly demagnified, but approaches the average magnification as it moves far away. Right: Total magnification as a function of source position for a random field of stars. Blue corresponds to de-magnification, and red to magnification, from average. The network of caustics allows for the production of many more micro-minima. Image courtesy of Dr. Wambsganss.

3.2 The search for micro-images

3.2.1 Background and Previous Work

Finding all the micro-images within a random star field of a given point source can be computationally intensive, as it involves finding all roots of the lens equation. For the lens equation as we have first presented it (as a function of vector variables $\vec{y}$ and $\vec{x}$), we would agree with Paczynski's [12] statement that within some circular region of radius r_{image}, "We are not aware of any theoretical criterion that would tell us that all micro-images within r_{image} have been found." However, Witt [21] and others have developed a lensing formalism in terms of complex variables. Such a shift has benefits (which we will put off until Chapter 5), and detriments, which we mention here.

Defining $w = y_1 + i \cdot y_2$ and $z = x_1 + i \cdot x_2$, the lens equation can be written as

$$w = z + \gamma\overline{z} - \sum_{i=1}^{n} \frac{1}{\overline{z} - \overline{z_i}}$$

where again we have taken all the stars located at the z_i to be of one unit mass that determines our unit distance, and as usual the overbar denotes conjugation. The lens equation in this form is not analytic, and so does not lend itself to some of the techniques of complex analysis for finding roots.[1] However, Witt has shown that the equation can be manipulated and a polynomial in $\overline{z}$ can be obtained, which is of order $n^2 + 1$ for $\gamma = 0$ or $(n+1)^2$ for $\gamma \neq 0$.[2] All roots of the lens equation are roots of this polynomial, but the converse is not true.

The fact that many stars in a field have a saddle point "associated" with their position allows one to use the locations of the stars plus a small perturbation as starting points in the search for micro-images, easily finding anywhere between n and $2n$ roots (the locations of the stars are technically roots of the lens equation, formally producing infinitely demagnified micro-maxima) of the lens equation. However, in regions sufficiently "close" to the location of the macro-image, the presence of stars can result in multiple extra image pairs of micro-minima and saddles. [3] Determining the locations of these micro-images is more difficult, as there is no approximate starting location to begin. Paczynski initially did so with a brute force grid search [12]. This is not guaranteed to find all images though, and for many images you may need a sufficiently dense grid to do so.[4]

Witt's polynomial in $\overline{z}$ theoretically allows one to obtain all roots of the lens equation without missing any. After such straightforward searches as just mentioned have been done (providing $\approx n$ to $\approx 2n$ roots), we are still left with $\approx n^2$ roots to find in Witt's polynomial. In a field consisting of thousands of stars the computational work required can still be very great and the time to find all these roots is prohibitively

[1] We will discuss such methods in Chapter 5 for finding the locations of critical curves and caustics.

[2] We do not present this polynomial here, as it is unnecessarily lengthy and is not used by us. The interested reader can find it in [21]. Simply knowing the number of roots suffices for our discussion.

[3] A more precise idea of just how close is "close" is provided later.

[4] As the author avoided using this method, exactly how dense a grid is sufficient is unclear.

large. Additionally, as Witt points out, not all of the solutions to his modified polynomial roots correspond to solutions of the lens equation [21]. The manipulations done to achieve a polynomial in $\overline{z}$ introduce extraneous solutions for z that are not necessarily solutions of the lens equation as well. For a system with n point masses and external shear, the maximum number of micro-images possible is much less - specifically, $5n - 1$ [1]. This means that to be sure you have found all micro-images, you are likely to waste as much (or more!) time finding extraneous roots which are then ignored.

The computational time and difficulty initially associated with finding micro-image locations has left the search for micro-images behind that of the development of IRS and IPM methods. Given that IRS and IPM methods allow one to more easily make statistical statements about the distributions of total magnifications (which is what we actually observe), the focus on their usage makes sense. However, as stated in the introduction, regions of interest occur when a pair of micro-images is created and the net flux is dominated by their contribution.

Improvements in both hardware and computational methods have now made determining the locations of micro-images less time intensive than it previously was however. The analysis of observed micro-lensing events can benefit greatly from understanding the properties of individual micro-images. Knowledge of the strengths of caustic crossings and how individual micro-images behave leading up to, during, and after an annihilation or creation can be illuminating.

3.2.2 Improvements made

Witt [22] and Lewis et. al. [8] present equivalent methods for calculating lightcurves of microlensed sources that move along a track in the source plane. Their method may be extended to finding the positions of the micro-images for a stationary point-source.

In essence, Witt and Lewis's lightcurve calculations rely on the fact that the image of an (ideally infinite) line in the source plane is comprised of a distorted line in the image plane with additional closed loops passing through every star, as seen in figure 3-2. A proof of this fact is outlined in both [8] and [13].

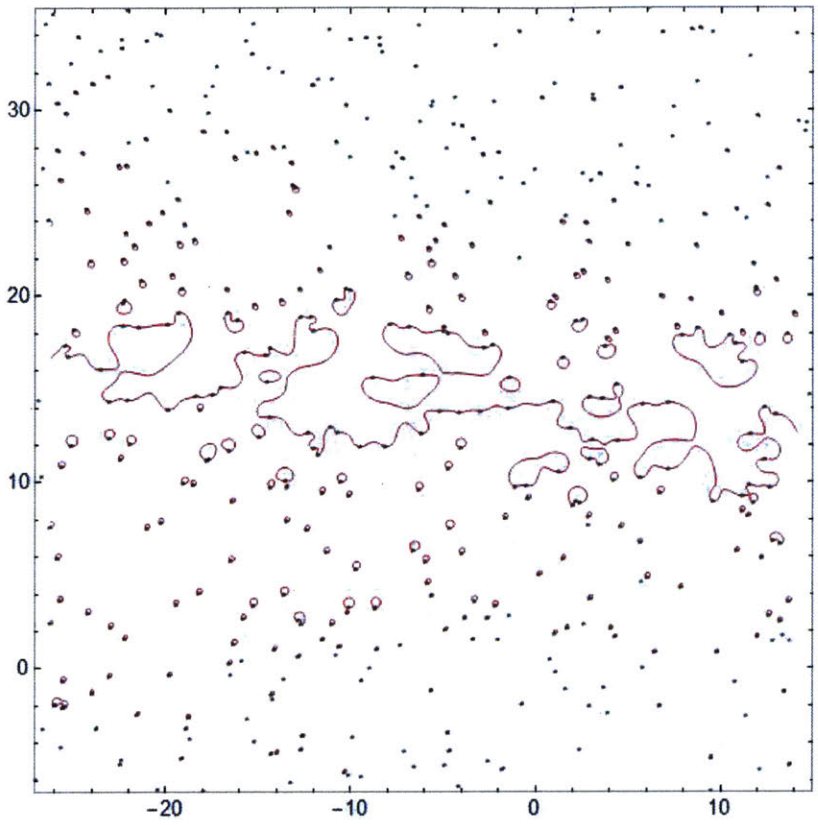

Figure 3-2: Images of a 1-dimensional linear source
As noted in [8], the images of an ideal infinite linear source are comprised of a distorted line in the image plane with additional closed loops (both represented here in red) that pass through at least one star (represented here by black dots). The stars on the edges of the field have loops passing through them as well which are much smaller, invisible at the scaling shown here.

Lewis's method for finding all the loops starts by following the image of the line far away from the field of stars, where it is near the expected location of the image of a line unperturbed by stars, and numerically following it towards, through, and back out of the field of stars.[5] Then, the loops around each stars are found using the location of the stars plus a small perturbation. This method effectively amounts to

[5]While an ideal starfield is taken to cover infinite area, simulations must obviously deal in a finite number of stars (and in reality, stars in a galaxy are finite as well). A large enough field is usually sufficient to derive important statistical properties, so long as it is big enough that edge effects can be ignored (for discussion on how many stars are enough, see [15]). This allows one to take advantage of the fact that you can place a source (be it a point or a line) far away from the caustics of a field of stars such that its macro-image is only slightly perturbed, and there are n micro-saddles associated with the n stars. As one moves the source towards the caustics, each caustic crossing will change the number of micro-images by two.

creating a contour plot for which $x_1 - (\nabla\phi)_1 - y_1 = 0$, where the lens equation is taken to be $\vec{y} = \vec{x} - \nabla\phi$ and the coordinate system is such that the track is parallel to the y_2 axis.

Modern computer algebra systems can now do this in a fraction of the time, though they may not find loops which are sufficiently small (as mentioned in figure 3-2). However, the images corresponding to these loops are micro-saddles which are not highly magnified, and so they contribute little to the lightcurve. If desired, a combination of contour plotting and a direct perturbative search near distant stars is effective.

A point source can be expressed as the intersection of two tracks, one with a constant y_1 value and the other with a constant y_2 value. The images of these two tracks will each consist of a perturbed line and loops in the image plane, which look different for each track. By taking the intersection of the set of images for each track, the locations of the micro-images are found for the point source located at the intersection of the tracks. The stars are automatically intersections of the set of images, for they are roots of the lens equation and must be contained in the loops for each track.

This process is mentioned in [15], although only for the case of modeling the locations of macro-images. Improvements in the ability to plot thousands of contours due to a large field of stars allows for the extension to micro-lensing.

Using Mathematica, the method essentially goes as follows, taking the lens equation to be of the form $\vec{y} = \vec{x} - \nabla\phi$:

1. Create a contour plot for which $x_1 - (\nabla\phi)_1 - y_1 = 0$. This plot will consist of loops around stars far away from the macro-image, and more complicated shapes as you get closer to the smoothed-out location of the macro-image.

2. Capture the list of all points used to make the contour plot. This will actually be a list of lists, where the outermost level is a list of the shapes/loops seen in the contour plot, and the inner level is the list of points used to create each of the shapes.

3. Calculate the sign of $x_2 - (\nabla\phi)_2 - y_2$ for every point $\vec{x}$ in the lists.

4. Wherever the sign of consecutive points changes from $+$ to $-$, or vice versa, a root of the lens equation is located. The points corresponding to the sign changes can be used as initial starting positions for further refinement using any numerical root-finding method.

As stated, this method is not guaranteed to find every micro-image as it is limited by the resolution of the contour plot you create. Mathematica (and presumably other computer algebra systems) have options to increase the number of initial points used to create contours, and adapt accordingly to create better plots. There are checks you can do to gain an idea of how correct this method is, and the author has been found it to be very reasonable.

One must pick a region to perform the search for micro-images in. The region must be large enough to include all micro-images of substantial magnification without missing any. For stars far away from the location of the macro-image, the associated micro-saddle points are highly de-magnified and vary as $\mu \propto r^{-4}$ [12]. Without requiring a high resolution, the contour plot method is likely to miss out on finding them. However, as previously noted, these saddle points are only slightly perturbed from the location of the stars, and so can be easily found using alternative methods. Micro-images that lie closer to the position of the macro-image will be substantially brighter, and it is finding the size of the region in which they lie that is more important.

The probability distribution for the deflection angle of a light ray passing through a field of stars has been calculated by Katz, Balbus, and Paczynski. For small values of the deflection angle α, [6] and [15] show that the probability distribution is approximately Gaussian with

$$p(\alpha) = \frac{1}{\pi\Delta} \cdot e^{-\alpha^2/\Delta}$$

where $\Delta = 2 \cdot \kappa_\star \cdot \ln(B\sqrt{N})$, $B = 2e^{1-\gamma} \approx 3.052$ (here $\gamma \approx 0.577$ is the Euler-Mascheroni constant, not the global shear), and N is the number of stars in the

field.[6] In the absence of global shear, the probability distribution is isotropic and depends only on the magnitude of the angle. However, "if the shear does not vanish, the observed positions of the microimages will not be isotropically distributed around the position of the macroimage" [6]. In this case, they are distributed in orthogonal directions (where one direction aligns with the external shear) with

$$\Delta_{\pm} = \frac{\Delta}{(1 - \kappa \pm \gamma)^2}$$

where κ is the total surface mass density and γ is the global shear [6].[7] The standard deviation of the Gaussian is equal to $\sqrt{\Delta/2}$ and is typically larger than 1, thus on the border of the regime wherein the approximation is valid. To be safe, we perform our searches in areas that lie within three standard deviations of the deflection angle around the location of the macro-image.

For regions near the location of the macro-image, a combination of our method with a magnification map proves extremely valuable. For a source located far away from the field of n stars, there will be n saddle points, plus one more additional saddle point or minimum depending on the macro-image. As the source moves closer to the field of stars, additional images are created/annihilated in saddlepoint/minimum pairs. From the magnification maps, one can determine how many images to expect based on the source location and the number of caustics separating it from a region of low magnification (no extra micro-minima present), and compare this with the number of images found using the contour plot. If there appear to be missing images, you can increase the sensitivity of the contours used to start and see how things change, or increase the size of the search region.

One of the biggest difficulties this method has is in separating micro-minima from micro-saddles at locations near the caustic after they emerge or shortly before they annihilate, when both micro-images are near each other. However, it is easy to start away from the caustic and trace backwards the locations of each image instead, as

[6] As discussed in [15], the presence of N in the distribution leads to interesting divergent results for an ideal infinite star field. Thankfully, in practice and reality all star fields are finite.

[7] As a reminder, we are using $\kappa_{dark} = 0$, so that κ here happens to be equal to $\kappa_{\star}$.

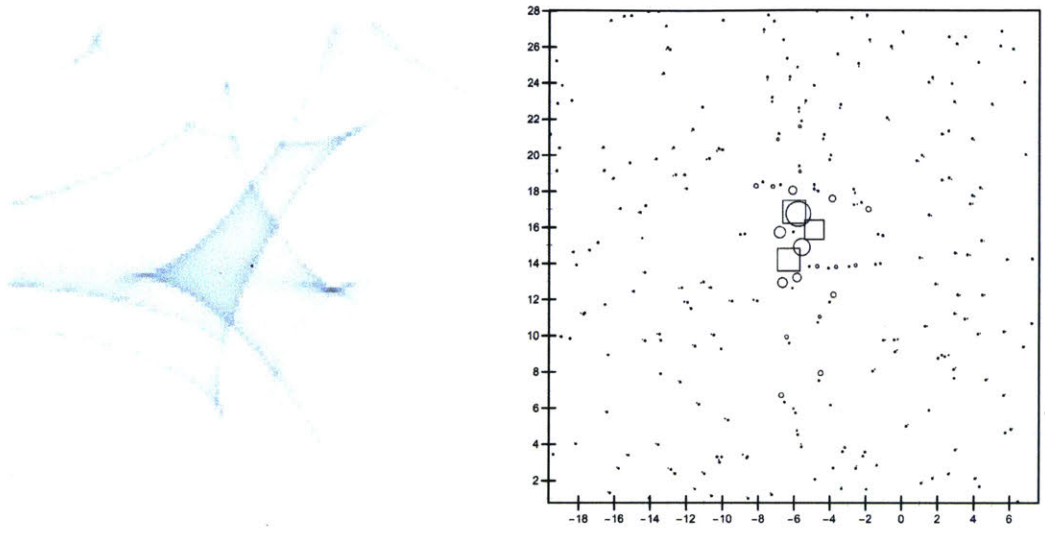

Figure 3-3: Source and micro-image positions
Left: Position of a point source (center, black dot) within a larger caustic network of a macro-saddle. While the magnification difference is not as obvious in gray-scale as a colored representation like figure 3-1 would show, it is still relatively easy to see that the source has three caustic crossings separating it from the de-magnified background, suggesting that there are 3 micro-minima present within its micro-images. Right: Positions of the micro-images that appear in a random star field due to a background point source located in the caustic network on the left. Micro-minima are represented as squares, and micro-saddles are circles. For dynamic range, the area of the micro-images scale logarithmically as the magnification, with $A(0) = 0$, $A(1) = 1$ in the units indicated.

Witt did in creating his lightcurves.

A visualization of the locations of the micro-images can be made after a search has been performed, as shown in figure 3-3. The point source is nearing a caustic, and is inside a region within which the caustics suggest there are 3 micro-minima. Simulations confirmed this, finding the presence of 3 micro-minima that are represented as squares in the right of figure 3-3. Saddlepoints are indicated by circles, and the areas of all the images scale logarithmically with their magnifications to provide a dynamic range showing many images. The search found approximately 83% of the expected number of micro-saddles, and the presence of them in the visualization suggests that the majority are of minimal magnification and any additional saddles would contribute little to the total magnification.[8]

[8]To be more precise, the saddles that were found range in magnification from ≈ 2 to $\approx 10^{-6}$,

The uppermost micro-minima is nearly concentric with a saddle point. This is the pair of images that will be annihilated as the source nears and crosses the caustic. They currently lie between magnification 1 and 10, but would greatly increase in magnification as the source moves closer to the caustic.

While not immediately apparent in the visualization, the micro-images tend to form a "train" that extends along the y-direction. This is due to the external shear working to stretch the images such that they would extend along that direction in the absence of micro-lensing stars (and hence producing the asymmetry in the distribution of the deflection angle for the two directions). For the particular system examined, we have that the standard deviations of the deflection angle for the x and y directions are 2.091 and 4.601 respectively. We can see that the majority of bright images lie within one standard deviation of the center of the visualization (which is centered on the position of the macro-image), and most certainly are contained within three standard deviations.

We come back once more to Paczynski's [12] note that "We are not aware of any theoretical criterion that would tell us that all microimages within r_{image} have been found." Lewis et. al. and Witt's method almost provides the way to do so. The limiting factor in being able to locate every micro-image is the resolution with which the closed loops of an ideal infinite linear source are created. With infinite resolution, one could check for sign changes as noted in item 4 of our method presented above, and thus know exactly where every image of a point source is located. However, with finite resolution one runs the risk of "jumping over" two consecutive roots which change the sign from $+$ to $-$, and then from $-$ to $+$ over a very small segment of a loop.

From our simulations, this seems most likely to happen due to source locations close to caustics, where the created micro-image pairs have nearly identical positions. If the expected distance between micro-images is greater than the resolution used to create the loops, we can expect most images to be found.

---

with the majority of order 10^{-3} or less.

3.3 Deviations of micro-image magnifications from the inverse square root approximation

3.3.1 Motivation

The magnification matrix can always be diagonalized and written in the form

$$\begin{pmatrix} 1-\gamma-S & 0 \\ 0 & 1+\gamma+S \end{pmatrix}$$

where S is the internal shear due to the stars. The magnification μ of each micro-image can be written as

$$\mu = \frac{1}{1-(\gamma+S)^2}.$$

For a micro-minimum, we know that

$$1-\gamma-S > 0$$
$$1+\gamma+S > 0$$

which, when combined with $\gamma > 0$, allows one to find that $0 < 1-(\gamma+S)^2 < 1$. Therefore, the magnification of a micro-minimum always satisfies $1 < \mu$. For source distances appropriately close to the caustic, a Taylor expansion of the magnification of each image in the created micro-image pair shows that $\mu \approx \frac{K}{\sqrt{d}}$, where we designate by K the strength of the caustic for a single image, and d is the source distance normal from the caustic crossing [15].[9] K^2 gives a sense of how far the source must travel for the created micro-minimum and saddle point to reach unit magnification. Clearly this approximation fails at some distance $d_{breakdown} > K^2$, as the micro-minimum must always stay above magnification 1.

[9]This approximation is for a *fold* caustic, i.e. one which can be approximated at some scale by a straight line. There are higher-order caustic events which are not discussed here. See [13], [15].

The coefficient K is equal to

$$K = \sqrt{\frac{1}{2 \cdot (\tau_{11})^2 \cdot \tau_{222}}}$$

in the coordinate system of the image plane, which is centered on the creation point of the micro-image pair, oriented such that $\tau_{12} = \tau_{22} = 0$, and evaluated at the image creation location [15]. More easily (in some cases) perhaps, Kayser and Witt have shown that this is equivalent to

$$K = \sqrt{\frac{1}{2|T|}}$$

where

$$T = A \cdot \begin{pmatrix} -\frac{\partial \det A}{\partial y} \\ \frac{\partial \det A}{\partial x} \end{pmatrix}.$$

A is again the inverse magnification matrix, and all evaluations are made at the location on the critical curve where the images appear [7]. We would like to note that the expressions here for K differ from what may be found elsewhere in the literature by a factor of two, as we are interested in the strength for a single micro-image whereas most references provide the strength for the net magnification, which takes into account both the minimum and saddlepoint of the created micro-image pair.

3.3.2 Caustic crossing for a Chang-Refsdal lens

For the single mass lens shown in figure 2-2, our source track moving along the y-axis crosses normal to the caustic at approximately $y = 1.039$. The strength at the corresponding image-pair creation position is found to be $K = 0.667$. We can then compare the approximation $\mu = \frac{0.667}{\sqrt{y-1.039}}$ against the actual micro-minimum magnification, although to be slightly more revealing we have instead examined $\log \mu$ vs. $\log \frac{d}{K^2}$ as shown in figure 3-4.

The solid line in the figure is that of the actual micro-minimum magnification, and the dashed line is that of the approximation. It is clear from the plot that, even for just a single perturbing star, the approximation is already broken at a strength-scaled

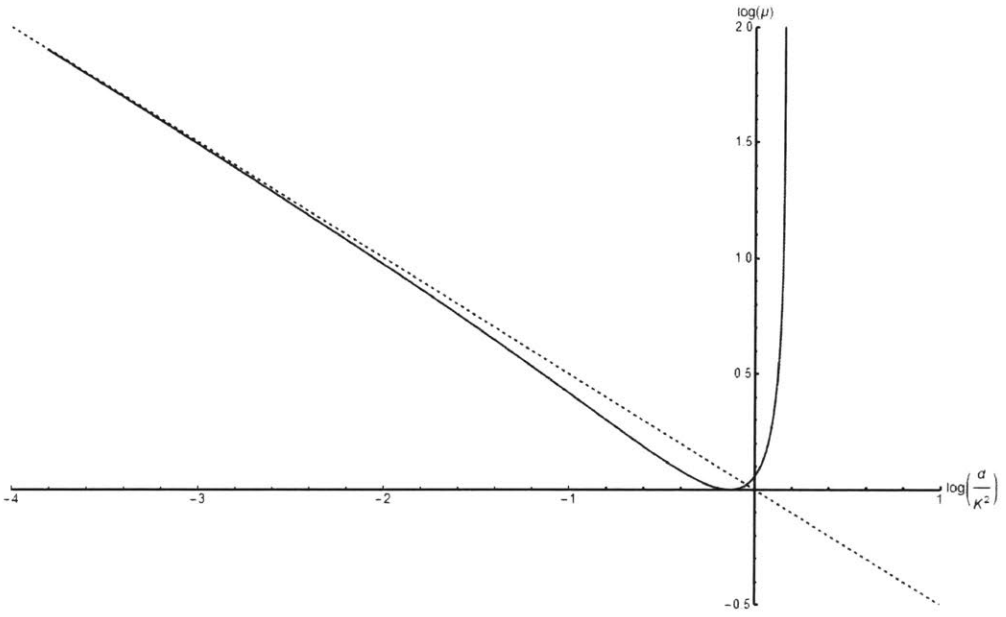

Figure 3-4: Log-log plot of magnification against distance from the caustic (scaled by caustic strength)
Magnification versus strength-scaled distance from the caustic for the micro-minimum of the lightcurve in figure 2-2. The solid line shows the magnification of the micro-minimum as a function of source position, and the dashed line shows the approximation $\mu = \frac{K}{\sqrt{d}}$.

distance from the caustic of 0.1, differing by a factor of approximately $\log \mu_{actual} - \log \mu_{approx} = -0.083$, or $\mu_{actual} = 0.826 \cdot \mu_{approx}$ at $\mu_{approx} = 10^{0.5} = 3.162$. It is interesting to note that in this case the actual magnification is lower than the approximation. In general, as will be seen, simulations suggest that magnifications tend to be higher than the approximation.

3.3.3 New results

Dr. Wambsganss provided star fields and magnification maps for the two cases of $\kappa = 0.73, \gamma = 0.72$ and $\kappa = 0.62 = \gamma$, which correspond to the saddle point macro-images of QSO 2237+0305 (Huchra's Lens). I was able to analyze the behavior of multiple micro-minima from their creation to their annihilation, as well the behavior of

their associated saddle points. Two randomly oriented tracks in the source plane were selected for each set of κ and γ. Using the magnification maps, positions along the tracks near caustics (on the side where extra micro-minima appeared) were identified. Given the source position close to the caustic, I was able to find the locations of micro-images and select the newly-created micro-minima and their companion saddle point. I was then able to iteratively track the position and magnification of these images as the source moved, from their creation to their annihilation (or in the case of many of the saddle points, until they were significantly de-magnified).

While Dr. Wambsganss's magnification maps don't provide exact locations of the caustics, by using the approximate source position, newly-created image pair position, and constraint that the source lie on the selected track, the exact caustic location can be numerically found along with the corresponding location on the critical curve. From these points the exact caustic strength can be calculated, as well as the angle between the source track and the normal to the caustic (which is needed to find the the distance normal from the caustic).

The two source tracks in each case provided ≈ 25 micro-minima in total for me to follow from creation to annihilation, thus providing ≈ 50 caustic crossing events to analyze. Log-log plots of magnification versus strength-scaled distance normal from the caustic are seen in figure 3-5. Note that each minima appears twice in the graph, not necessarily in the same color (a minimum that was the first present at its creation, but the third present at its annihilation, is seen in both red and green on the plot, as the annihilation is a creation in reverse). Additionally, the minimum has a different lifetime along the x-axis in each case as the caustics at either end have different strengths.

The plots in figure 3-5 reinforce the conclusion from examining the Chang-Refsdal lens that deviations from the approximation start to occur at small distances from the caustic (or equivalently at higher than unit magnifications). For the micro-minima that manage to make it a unit distance away from the caustic, the graphs show that their magnification is higher than unit by roughly $10^{0.2\pm0.2}$.

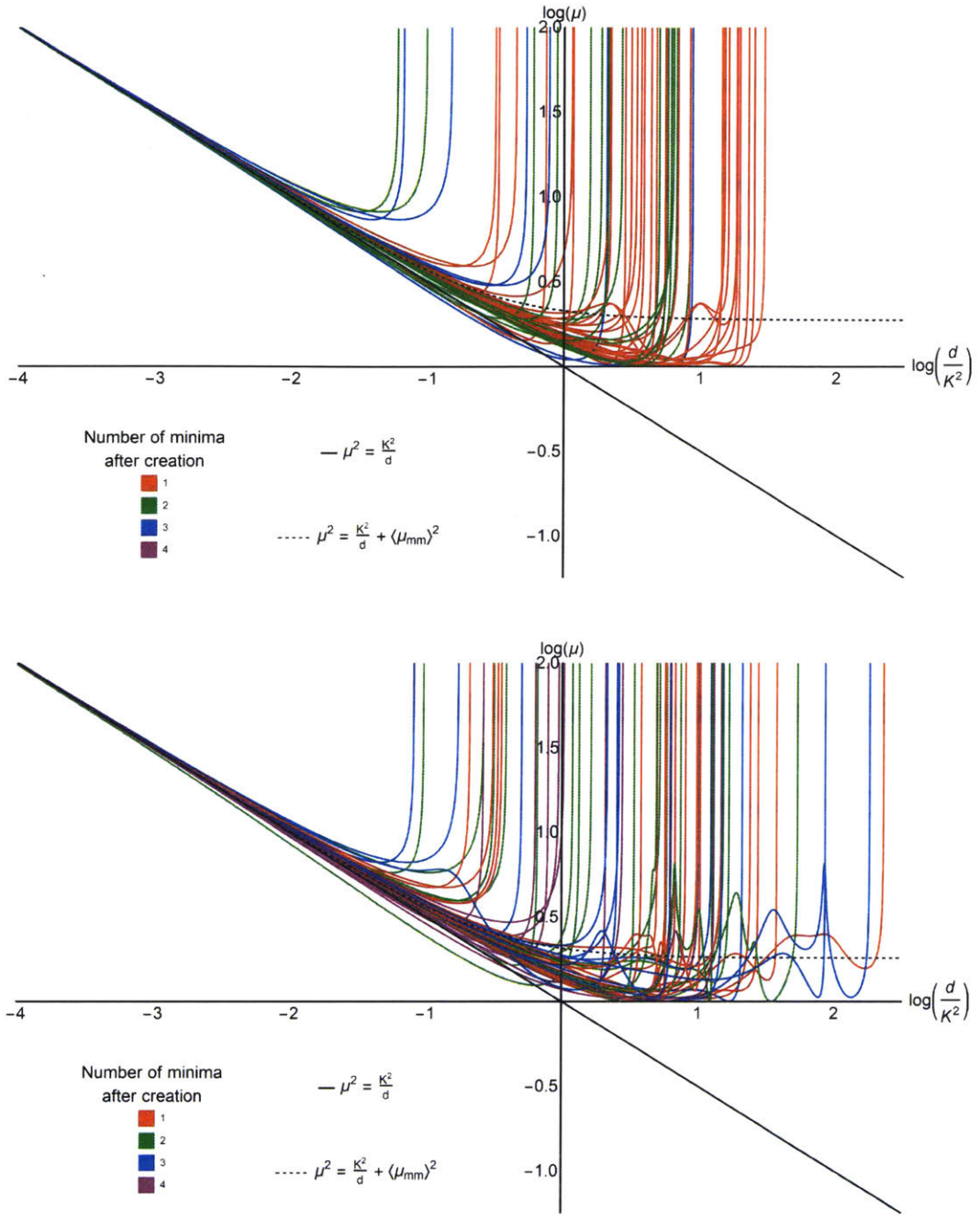

Figure 3-5: Magnification as a function of source distance (normalized by caustic strength) from the caustic for many micro-minima

Plots of $\log \mu$ vs. $\log \frac{d}{K^2}$. Top: $\kappa = 0.73, \gamma = 0.72$. Bottom: $\kappa = 0.62 = \gamma$. The colors denote whether the minimum was the first, second, third, or fourth present at its time of creation after the source crossed the caustic. The solid black line is $\mu = \frac{K}{\sqrt{d}}$, and the dotted black line is an alteration to the approximation discussed in Chapter 4.

Future alterations to the method

If the exact locations of the caustics are known, one can pick a point along a caustic and find the normal direction, thus allowing for the tracking of a micro-minimum from creation to annihilation along the proper track. At the annihilation end, the intersection of the track with the caustic is almost certainly not normal. However, the normal at the intersection point could be found and a new track could be started from there. This would allow one to "ping pong" or "bounce" along from caustic crossing to caustic crossing. However, this may not provide as random a sampling of minima creation numbers, or caustic regions, to explore as might be desired. Alternatively then, it may be best to randomly identify points that lie on the caustic, calculate the normal directions, and proceed from there to compile micro-minimum magnification information.

3.4 Distribution of caustic strengths

3.4.1 Two cases: $\kappa = 0.73$, $\gamma = 0.72$, and $\kappa = 0.62 = \gamma$

Normalizing the distances from the caustic required calculations of caustic strengths. The distributions for the strengths in the two cases analyzed can be seen in figure 3-6. The ≈ 50 strengths were binned into intervals of size 0.1.

3.4.2 Results

For $\kappa = 0.73$, $\gamma = 0.72$ the mean and standard deviation are 0.376 and 0.208 respectively. For $\kappa = 0.62 = \gamma$, the mean and standard deviation are 0.332 and 0.123 respectively.

Further simulations for many values of κ and γ would be necessary to gain a true understanding of how their variations change the distributions.

Witt has calculated statistics of caustic lengths and strengths for the case of no external shear, examining surface mass densities corresponding to macro-minima and maxima [21]. The cases studied here are for two macro-saddles, for which the

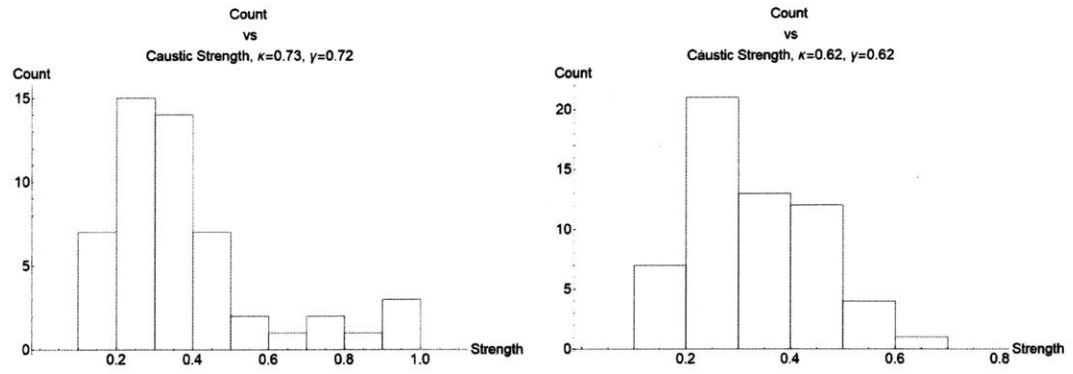

Figure 3-6: Histograms of caustic strengths
Distributions of the caustic strengths for the two cases examined of $\kappa = 0.73$, $\gamma = 0.72$ and $\kappa = 0.62 = \gamma$.

author is unaware of any calculations of similar parameters with which to compare. We present our own calculations later, and compare the samples here to the more precisely calculated probability distribution of caustic strengths in Chapter 5.

3.5 Relevance to observed events

In many analyses of caustic crossing events, the approximation that the magnification goes like the inverse of the square root of the source-caustic distance is used. Clearly this is not in actuality an ideal model for events.

As an example of the issue, Shalyapin et. al. [17] perform an analysis on the nature and size of the optical continuum source in QSO 2237+0305. In section 2.2, they derive expressions for the optical flux during a caustic crossing following the procedure of [16] and others. This procedure starts by multiplying the emission profile $I_s(x, y)$ of the source with an approximation of the magnification factor near a caustic as $\mu_{approx}(x, y) = \mu_0 + \dfrac{K \cdot H(x)}{\sqrt{x}}$.[10] The multiplication is then integrated over the source profile to give the net observed flux,

$$F_{obs} = \iint \mu(x, y) \cdot I_s(x, y)\, dxdy.$$

[10]The strength here is equal to twice what I have been considering in strength calculations, as mentioned due to the fact that there are two created micro-images which dominate the flux. $H(x)$ is the Heaviside function.

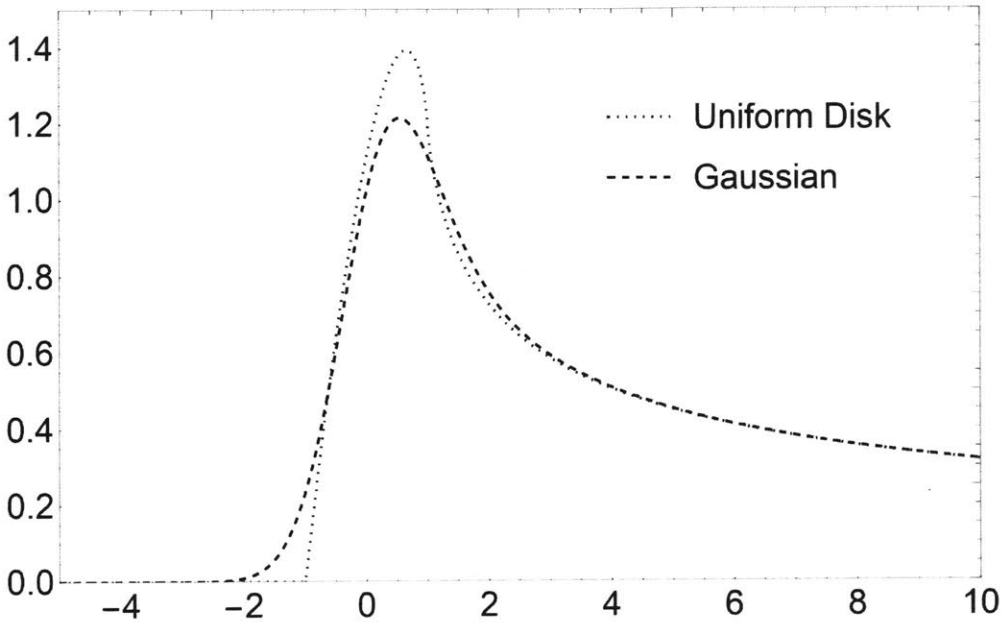

Figure 3-7: Sample lightcurve shape profiles for two different source profiles
A uniform disk and a Gaussian profile (as in [16]) produce the shape profiles seen here. Distances are from source center to caustic, in units of the caustic strength. Each has $R = 1$ for equations B3 and B8 of [16].

The integral splits into two parts. The first is equal to the net flux from the source F_s multiplied by the approximately constant magnification factor μ_0 due to all micro-images other than the created pair, and the second is that which varies with distance from the caustic. This second integral is the one of interest. As we have shown, the approximation appearing inside the integral due to μ is only valid for a small region near the caustic. If the emission profile of the source extends beyond this region, then we expect deviations between what the approximation gives and what the actual value should be.

The expression can be written as $F_{obs}(d) = \mu_0 \cdot F_s + F_c \cdot J(d)$ where F_c is a constant which is proportional to the caustic strength, and $J(d)$ determines the shape of the profile as a function of distance from the center o the source to the caustic. For two sample sources of a uniform disk and a Gaussian, [16] and [17] show what the shapes of J would look like as a function of source position. Such profiles are shown in figure 3-7.

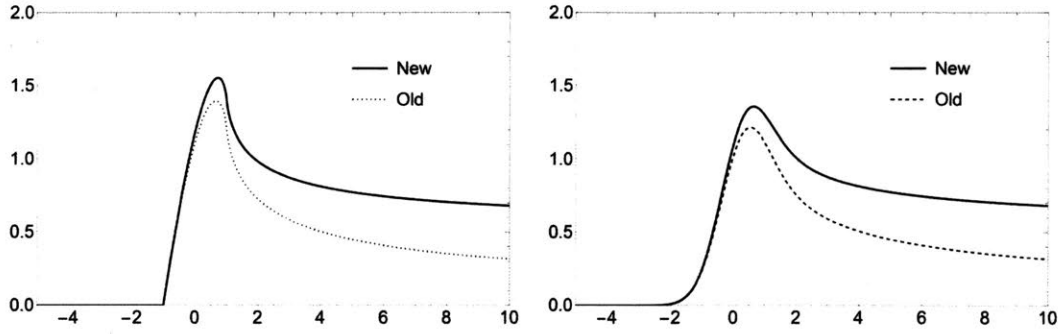

Figure 3-8: Modified lightcurve shape profiles
Left: Uniform circular disk. Right: Gaussian. Bold lines indicate the modified approximation, dotted and dashed lines indicate the ones used in [16] and [17], as shown in figure 3-7.

Each shares roughly the same qualitative features. However, the important fact to note is stated in [16]: "Note the assymmetry of $J(d)$...a turning point at $d \approx 1$ and then it approaches the asymptotic $d^{-1/2}$ behavior." As our simulations show, by the time $d = 1$ has come around, the approximation used for the magnification has already been broken at a tenth of the distance. Thus the shape profiles must be incorrect.

As a toy examination of how alterations to the approximation change the shape of the profile, for the micro-minimum one could take the approximation to instead have the form $\mu = \sqrt{\frac{1}{x} + 1}$. While not deeply motivated, this form has the property that it goes to 1 as $d \to \infty$, as desired. Additionally, at $d = 1$, $\log \mu = 0.150$, which is approximately the average value at which most micro-minima that make it past $d = 1$ cross the $\log \mu$ axis in figure 3-5. The saddlepoint can be left unmodified, as it is allowed to be infinitely demagnified. This leads to the change

$$\mu_{approx}(x, y) = \mu_0 + \frac{K \cdot H(x)}{2}\left(\sqrt{\frac{1}{x} + 1} + \frac{1}{\sqrt{x}}\right).$$

The modified shape profiles due to this change can be seen in figure 3-8. The modification preserves the same general shape of the profile. However, the shape tends to have a higher peak, is slightly more extended, and levels out to a higher value (as is expected, since the micro-minimum must stay at magnification 1 or greater).

Shalyapin et. al. use the shapes of figure 3-7, along with a few other source profiles, to match the observed lightcurves of QSO 2237+0305 and determine parameters of the system [17]. The brief examination above suggests that the change in the shape profile J has the effect of decreasing the fitted value of F_c appearing in [17] in order to produce the same net $F_{opt}(t) \equiv F_{obs}$. The conclusion that a standard source model is the best fit may then no longer be the case. Additionally, the change to J may suggest a decrease in the caustic crossing time Δt that was fit to the data, possibly affecting the estimated velocity or the size of the emitting region.

In brief then, models used to analyze caustic crossing events do not properly take into account the difference in behavior between the micro-minimum and micro-saddle that form the created image pair. Deviations from the magnification approximation suggest the need for some form of alteration. A model that fits caustic crossings better than the $\frac{1}{\sqrt{d}}$ approximation would allow for more correct analyses of caustic crossing events.

Chapter 4

Statistics for Micro-Minimum Magnifications

4.1 Mean micro-minima magnification

4.1.1 From mean number of micro-minima to mean micro-magnification

The alteration $\mu(x) = \sqrt{\frac{1}{x} + 1}$ for a micro-minimum has the magnification of the minimum decay down to its smallest possible value of 1. However, one might expect that there is an average value a micro-minimum may tend to which is not necessarily equal to 1.

Granot, Schechter, and Wambsganss have performed calculations regarding the mean number of micro-minima present in a macro-image [5], based upon earlier work done by Wambsganss, Witt, and Schneider [19]. Their calculation can be extended to find the mean magnification of each of these micro-minima.

The magnification of an image can be expressed as an area ratio between the image and source. Suppose the macro-image of a lensed source is comprised of micro-images, of which the micro-minima take up an area A_d. A small area dA_d for which the magnification μ is approximately constant over the extent of the area gets mapped to an area dA_s in the source plane with the relation $dA_s = dA_d/\mu$.

As discussed in [5], the magnification at a point can be written as

$$\mu^{-1} = 1 - (\gamma + S_1)^2 - S_2^2,$$

where the coordinate system is aligned with the external shear, and S_1 and S_2 are then the shear contributions due to the micro-lensing stars. We have again taken $\kappa_{dark} = 0$, and as noted in [5] the convergence due to the stars disappears everywhere except at the locations of the stars.

Following the analysis of [5], the area $dA_d = A_d \cdot p(\kappa_\star, S_1, S_2) \cdot dS_1 dS_2$ in the image plane is mapped to an area $dA_s = dA_d/\mu(\gamma, S_1, S_2)$ in the source plane. Here, $p(\kappa_\star, S_1, S_2)$ is the probability distribution of the shear (the actual underlying variable that changes with position, as it determines the magnification), which was calculated by Nityananda and Ostriker and is found from [11] or [15] to be equal to

$$p(\kappa_\star, S_1, S_2) = \frac{1}{2\pi} \frac{\kappa_\star}{(\kappa_\star^2 + S_1^2 + S_2^2)^{3/2}}.$$

The mean micro-minimum magnification $\langle \mu_{mm} \rangle$ is then found by

$$\langle \mu_{mm} \rangle = \frac{\iint_{\mu>0} dA_d}{\iint_{\mu>0} dA_s} = \frac{\iint_{\mu>0} dA_d}{\iint_{\mu>0} \frac{dA_d}{\mu(\gamma, S_1, S_2)}}$$

$$\langle \mu_{mm} \rangle = \frac{\iint_{\mu>0} p(\kappa_\star, S_1, S_2)\, dS_1\, dS_2}{\iint_{\mu>0} \frac{p(\kappa_\star, S_1, S_2)}{\mu(\gamma, S_1, S_2)}\, dS_1\, dS_2}.$$

The denominator is an expression calculated in [5], namely the mean number of positive-parity micro-images divided by the mean macro-magnification.

In light of that, the expression for $\langle \mu_{mm} \rangle$ can be rewritten as

$$\langle \mu_{mm} \rangle = \frac{\langle \mu_{macro} \rangle}{\langle N \rangle} \cdot p(\mu(\kappa_\star, S_1, S_2) > 0),$$

where $p(\mu(\kappa_\star, S_1, S_2) > 0)$ denotes the probability that random shear from the star field produces a micro-minimum at a point as opposed to a micro-saddle.

The value of $\langle \mu_{mm} \rangle$ can be viewed as taking the macro-magnification, which consists of both micro-minima AND micro-saddles, multiplying by the probability that random shear produces a minimum instead of a saddle point, and dividing by the mean number of micro-minima.

There exist expressions for the integrals in the numerator and denominator (as partially shown in [5]), which can be numerically evaluated over the range of S_1 and S_2 which produce micro-minima. However, a somewhat easier one dimensional expression can be found using $p(\mu)$ from equations 11.63*a*, 11.63*b*, and 11.63*c* of [15], producing

$$\langle \mu_{mm} \rangle = \frac{\int_1^\infty p(\mu)\, d\mu}{\int_1^\infty \frac{p(\mu)}{\mu}\, d\mu}.$$

4.1.2 Values for mean micro-minima magnifications

The values of $\langle \mu_{mm} \rangle$ for a range of $\kappa_\star$ and γ values are listed in table 4.1.

As noted by Granot, Schechter, and Wambsganss, when $\kappa_\star = 0$, there are no extra micro-images [5]. For the range of γ values displayed, there is only one image which is a minimum. The magnification of this must be equal to $\frac{1}{1-\gamma^2}$.

It is also worth pointing out that in the top row where $\gamma = 0$, $\langle \mu_{macro} \rangle \to \infty$ as $\kappa \to 1$. However, the mean number of micro-minima and the shear probability combine in such a way that the average magnification of a single micro-minimum is finite.

The values of $\langle \mu_{mm} \rangle$ as found in table 4.1 can be used to alter the approximation for the magnification of a micro-minimum near a caustic. Instead of adjusting such that $\mu(x) = \sqrt{\frac{1}{x} + 1}$, which decays down to 1, we can take $\mu(x) = \sqrt{\frac{1}{x} + \langle \mu_{mm} \rangle^2}$.

For the values of $\kappa_\star$ and γ used in our simulations, we find that $\langle \mu_{mm} \rangle = 1.880$ for $\kappa_\star = 0.73$, $\gamma = 0.72$ and $\langle \mu_{mm} \rangle = 1.803$ for $\kappa_\star = 0.62 = \gamma$. These approximations have been included as the dotted lines in figure 3-5. In general, the estimate lies on the high

$$\langle \mu_{mm} \rangle = \frac{\langle \mu_{macro} \rangle}{\langle N \rangle} \cdot \text{p(shear produces a micro-minimum)}$$

γ	$\kappa_\star = 0$	0.001	0.003	0.01	0.03	0.1	0.3	0.5	0.7	0.9	0.97	0.99	0.997	0.999	1
0	1.000	1.001	1.003	1.010	1.030	1.100	1.287	1.447	1.573	1.669	1.696	1.704	1.706	1.707	1.707
0.001	1.000	1.001	1.003	1.010	1.030	1.100	1.287	1.447	1.573	1.669	1.696	1.704	1.706	1.707	1.707
0.003	1.000	1.001	1.003	1.010	1.030	1.100	1.287	1.447	1.573	1.669	1.696	1.704	1.706	1.707	1.707
0.01	1.000	1.001	1.003	1.010	1.030	1.100	1.287	1.447	1.574	1.669	1.696	1.704	1.706	1.707	1.707
0.03	1.001	1.002	1.004	1.011	1.031	1.100	1.288	1.448	1.574	1.669	1.696	1.704	1.706	1.707	1.707
0.1	1.010	1.011	1.013	1.020	1.040	1.110	1.298	1.456	1.580	1.674	1.700	1.707	1.710	1.711	1.711
0.3	1.099	1.100	1.102	1.110	1.131	1.203	1.384	1.526	1.631	1.709	1.732	1.738	1.740	1.740	1.741
0.5	1.333	1.335	1.337	1.345	1.367	1.439	1.584	1.671	1.731	1.777	1.791	1.795	1.796	1.796	1.796
0.7	1.961	1.962	1.963	1.969	1.983	2.003	1.944	1.889	1.868	1.866	1.868	1.869	1.869	1.869	1.869
0.9	5.263	5.245	5.207	5.074	4.683	3.575	2.437	2.130	2.011	1.959	1.950	1.947	1.946	1.946	1.946
0.97	16.921	16.480	15.637	13.076	8.575	4.318	2.574	2.200	2.055	1.989	1.976	1.973	1.972	1.971	1.971
0.99	50.251	44.870	36.374	20.676	9.591	4.408	2.604	2.217	2.066	1.997	1.983	1.980	1.979	1.978	1.978
0.997	166.917	106.235	56.880	21.821	9.530	4.418	2.613	2.223	2.070	2.000	1.986	1.982	1.981	1.981	1.980
0.999	500.250	147.249	57.397	21.238	9.460	4.419	2.615	2.225	2.072	2.001	1.986	1.983	1.982	1.981	1.981
1	∞	130.770	53.099	20.774	9.416	4.419	2.616	2.225	2.072	2.001	1.987	1.983	1.982	1.982	1.981

Table 4.1: Mean micro-minimum magnifications for varying convergence and shear

Values of $\langle \mu_{mm} \rangle$ for a range of convergence and shear. For $\kappa_\star = 0$, there is only one image whose magnification is equal to that of the macro-image (as the range of shear values only produce minima). For $\gamma = 0$, as $\kappa_\star \to 1$, $\langle \mu_{macro} \rangle \to \infty$. However, the mean number of micro-minima and the shear probability combine such that $\langle \mu_{mm} \rangle$ is finite. The gray boxes along the diagonal mark the values of $\kappa_\star$ and γ which correspond to $\langle \mu_{macro} \rangle = \infty$. Macro-minima lie above the diagonal, while macro-saddles lie below.

end for the micro-minima which manage to make it to $\frac{d}{K^2} = 1$, and continues to be an increasingly worse over-estimate as $\frac{d}{K^2}$ increases. However, the fact that the function levels out means the difference between approximation and actual value is still better than the original un-adjusted approximation at increasingly larger distances.

Table 4.2 presents values of $\langle \mu_{mm} \rangle$ for a range of $\kappa_\star$ and $\langle \mu_{macro} \rangle$. Table 4.3 provides the mean number of micro-minima $\langle N \rangle$ for the same parameters. Together, $\langle N \rangle$ and $\langle \mu_{mm} \rangle$ give a sense of what proportion of $\langle \mu_{macro} \rangle$ is due to micro-minima, and can indirectly also provide an idea of what proportion may be due to micro-saddles. For example, examining $\langle \mu_{macro} \rangle = 30$ and $\kappa_\star = 0.3$, we see that $\langle \mu_{mm} \rangle = 1.890$ and $\langle N \rangle = 9.444$. This suggests that in total the micro-minima provide a magnification of 17.849. The remaining magnification comes from the micro-saddles, which can be placed into two categories: those which would exist anyways due to the presence of micro-lenses (the associated saddle points), and those due to the creation of extra micro-minima (as the "ground state" would contain only the minimum which is associated with the macro-minimum). On average, for this case there are 8.444 micro-saddles which come from the extra image pairs (one less than the mean number of micro-minima, as our macro-image is a minimum and thus starts out with one micro-minimum).

If we assume that the extra-image pairs lie within an ellipse whose semi-major and semi-minor axes are given by $\sqrt{\Delta_\pm/2}$ as discussed in Chapter 3, we can place rough bounds on the average magnification of the extra saddle points.

An upper bound on their average magnification would be to take the remaining magnification of $30 - 17.849 = 12.151$ distributed evenly between all 8.444 saddles, for an average magnification of 1.794 for each of the extra saddles.

A very rough lower bound can be found as follows. We expect $\kappa_\star \cdot \frac{A}{\pi}$ stars to lie within the ellipse, each of which is assumed to have an associated saddle point. The number of saddles then reduces to

$$N_s = \frac{1}{2}\kappa_\star \cdot \sqrt{\Delta_+}\sqrt{\Delta_-} = \frac{1}{2}\kappa_\star \cdot \Delta \cdot |\langle \mu_{macro} \rangle| = \kappa_\star^2 \cdot |\langle \mu_{macro} \rangle| \cdot \ln(B\sqrt{N}).$$

$$\langle \mu_{mm} \rangle = \frac{\langle \mu_{macro} \rangle}{\langle N \rangle} \cdot \text{p(shear produces a micro-minimum)}$$

μ_{macro}	$\kappa_\star = 0$	0.001	0.003	0.01	0.03	0.1	0.3	0.5	0.7	0.9	0.97	0.99	0.997	0.999	1
3	3	2.981	2.943	2.820	2.533	1.961	1.463	-	-	-	-	-	-	-	-
10	10	9.693	9.136	7.633	5.326	2.951	1.786	1.579	-	-	-	-	-	-	-
30	30	26.817	22.147	13.969	7.308	3.357	1.890	1.640	1.610	-	-	-	-	-	-
100	100	67.627	41.302	18.522	8.193	3.509	1.927	1.662	1.625	-	-	-	-	-	-
300	300	112.668	51.845	19.993	8.449	3.553	1.938	1.668	1.629	1.672	-	-	-	-	-
1000	1000	138.382	55.560	20.478	8.537	3.569	1.942	1.670	1.631	1.673	-	-	-	-	-
3000	3000	144.854	56.469	20.611	8.562	3.573	1.943	1.671	1.631	1.673	1.696	-	-	-	-
-3000	-	148.706	57.255	20.740	8.587	3.578	1.944	1.671	1.631	1.674	1.697	1.704	1.706	1.707	1.707
-1000	-	147.342	57.878	20.865	8.612	3.582	1.945	1.672	1.632	1.674	1.697	1.704	1.706	1.707	1.707
-300	-	94.846	58.080	21.268	8.698	3.598	1.949	1.674	1.633	1.675	1.698	1.705	1.707	1.708	1.708
-100	-	33.265	39.729	21.931	8.935	3.642	1.960	1.680	1.638	1.678	1.701	1.707	1.710	1.711	1.711
-30	-	12.928	13.975	16.304	9.532	3.796	1.998	1.702	1.652	1.689	1.710	1.716	1.719	1.719	1.720
-10	-	6.508	6.651	7.159	7.853	4.188	2.107	1.763	1.694	1.718	1.736	1.742	1.744	1.744	1.744
-3	-	3.693	3.710	3.769	3.931	4.029	2.453	1.967	1.832	1.814	1.820	1.822	1.823	1.823	1.823

Table 4.2: Mean micro-minimum magnifications for varying convergence and macro-magnification

Values of $\langle \mu_{mm} \rangle$ for a range of convergence and macro-magnification. Not all values of $\kappa_\star$ shown can produce the $\langle \mu_{macro} \rangle$ indicated, thus the absence of values in the upper right corner. For $\kappa_\star = 0$, there are no extra micro-images. Therefore, the value for $\langle \mu_{mm} \rangle$ is equal to that of the macro-minimum, or non-existant for a macro-saddle.

$\langle N \rangle$															
μ_{macro}	$\kappa_\star = 0$	0.001	0.003	0.01	0.03	0.1	0.3	0.5	0.7	0.9	0.97	0.99	0.997	0.999	1
3	1	1.004	1.012	1.040	1.110	1.283	1.396	-	-	-	-	-	-	-	-
10	1	1.025	1.073	1.233	1.628	2.555	3.458	3.284	-	-	-	-	-	-	-
30	1	1.098	1.286	1.885	3.267	6.342	9.444	9.186	7.742	-	-	-	-	-	-
100	1	1.399	2.138	4.339	9.155	19.68	30.43	29.87	25.29	-	-	-	-	-	-
300	1	2.356	4.715	11.47	26.04	57.81	90.41	88.97	75.42	59.21	-	-	-	-	-
1000	1	5.865	13.88	36.51	85.19	191.3	300.3	295.8	250.9	197.0	-	-	-	-	-
3000	1	16.01	40.11	108.1	254.2	572.6	900.1	886.8	752.2	590.8	534.0	-	-	-	-
-3000	0	14.52	38.63	106.6	252.8	571.4	899.3	886.2	751.8	590.5	536.7	521.9	516.8	515.3	514.6
-1000	0	4.385	12.39	35.06	83.80	190.1	299.5	295.2	250.5	196.7	178.8	173.9	172.2	171.7	171.5
-300	0	0.985	3.249	10.02	24.66	56.59	89.53	88.33	74.98	58.92	53.56	52.08	51.57	51.43	51.36
-100	0	0.231	0.778	2.901	7.77	18.46	29.55	29.23	24.85	19.54	17.77	17.28	17.11	17.07	17.04
-30	0	0.045	0.142	0.555	1.899	5.129	8.563	8.552	7.303	5.763	5.246	5.103	5.054	5.039	5.032
-10	0	0.009	0.028	0.099	0.364	1.354	2.578	2.650	2.295	1.829	1.670	1.626	1.610	1.606	1.604
-3	0	0.001	0.004	0.013	0.042	0.181	0.529	0.611	0.559	0.462	0.427	0.417	0.413	0.412	0.412

Table 4.3: Mean number of micro-minima for varying convergence and macro-magnification
Values of $\langle N \rangle$ for a range of convergence and macro-magnification. Not all values of $\kappa_\star$ shown can produce the $\langle \mu_{macro} \rangle$ indicated, thus the absence of values in the upper right corner. For $\kappa_\star = 0$, there are no extra micro-images. Therefore, the value for $\langle N \rangle$ is equal to 1 for a macro-minimum, and 0 for a macro-saddle.

For $\langle \mu_{macro} \rangle = 30$ and $\kappa_\star = 0.3$, we have that

$$N_s = 2.7 \ln 3.052 \sqrt{N}.$$

For $N = 10^3$, 10^4, and 10^5 (approximately the orders of magnitude for star fields used in micro-lensing ray tracing simulations), we have that $N_s = 12.34$, 15.45, and 18.56 respectively. Combined with the saddle points of the extra image pairs, this produces average magnifications of 0.585, 0.509, and 0.450 respectively. These values are not very strict for two reasons. We have ignored the magnifications of the associated saddle points outside of our ellipse, although we expect their contribution to be a small portion of the total magnification. Additionally, we assume that the magnification not due to micro-minima is evenly distributed among the saddles within the ellipse. It is more likely that saddles closer to the location of the macro-image are brighter, and saddles closer to our elliptical boundary are slightly dimmer. However, we can see at least from the upper bound that the micro-saddles are on average less magnified than the minima (which is expected).

4.2 Extension to distributions for caustic strengths

For a micro-lensing system with no external shear, the magnification matrix can be put in the form

$$A = \begin{pmatrix} 1 - S_1 & S_2 \\ S_2 & 1 + S_1 \end{pmatrix}$$

where $1 - S_1 = \dfrac{\partial^2 \tau}{\partial x_1^2}$, $1 + S_1 = \dfrac{\partial^2 \tau}{\partial x_2^2}$ and $S_2 = \dfrac{\partial^2 \tau}{\partial x_2 \partial x_1}$ are the contributions to the shear due to the field of stars. The coordinate system can always be rotated such that $S_2 = 0$.

For a point on a critical curve, one of the eigenvalues $1 + S_1$ or $1 - S_1$ must vanish (the choice is arbitrary and simply defines a coordinate system at the particular critical point). Taking $1 + S_1 = \tau_{22} = 0$ as in [15], the formula for the caustic strength

becomes

$$K = \sqrt{\frac{1}{2 \cdot (\tau_{11})^2 \cdot \tau_{222}}} = \sqrt{\frac{1}{8 \cdot \tau_{222}}}$$

in the coordinate system of the image plane, which is centered on the creation point of the micro-image pair, and where all evaluations happen at the image creation location [15].

Schneider, Ehlers, and Falco provide calculations for the probability distributions of the deflection angles, as well as for the shear [15]. As the deflection angle is proportional to the first derivatives of the potential, and the shear is proportional to second derivatives, it is reasonable to question whether such distributions can also be found for third derivatives of the potential.

The steps to do so will be outlined here, although we were unable to approximate or simplify the expressions derived.

Following the procedure outline in [11] and [15] for calculating the probability distributions for the shear, the probability density for the third derivative of the potential of interest to us is given by

$$p(Z) = \frac{1}{2\pi} \int Q_N(t) \cdot e^{-i \cdot t \cdot Z} dt$$

where Z denotes our variable of interest, $Q_N(t) = (q(t))^N$, and

$$q(t) = \frac{1}{\pi R^2} \int_0^R \int_0^{2\pi} e^{i \cdot t \cdot g(r,\theta)} r d\theta dr.$$

R is the size of the star field, N is the number of stars in the field (both of which are eventually taken to ∞ while keeping $\kappa_\star$ constant), and

$$g(r, \theta) = \frac{-2 \cos\theta \cdot (\cos^2\theta - 3\sin^2\theta)}{r^3}$$

is the contribution to the third derivative of the potential due to a single star located at (r, θ).

The first difficulty encountered is evaluating the integral over θ for $q(t)$. In the calculation of the probability distribution $p(S)$ for the shear, the integral takes a

slightly different form that is able to be expressed in terms of Bessel functions, which can be further integrated and approximated to ultimately solve for $p(S)$. We had no quick luck in doing so for $p(Z)$, but future work may make the evaluation possible. Until then, strength distributions must be calculated empirically as done by Witt [21].

Chapter 5

Determining the locations of critical curves and caustics

5.1 Background

Witt and others developed a lensing formalism in terms of complex variables, as opposed to vector variables $\vec{y}$ and $\vec{x}$ [21]. Such a change allows for a parametric representation of the critical curves of a field of stars, which can then be mapped through the lens equation to get the caustic network. Such a process allows for calculations of the probability distributions of the strength of caustics. Witt did so for a range of convergence values, while ignoring external shear. We have been unable to find similar work examining distributions for systems with external shear. As we do not have access to Witt's code for the work that he did, we present our own method of finding the locations of the critical curves and caustics and hence the distributions of caustic strength.

5.2 A switch to complex variables

The necessary equations for us have been outlined by Witt already, and we will simply present them here [21]. Let $w = y_1 + i \cdot y_2$ and $z = x_1 + i \cdot x_2$. Then the lens equation

takes the form

$$w = z + \gamma\overline{z} - \sum_{i=1}^{n} \frac{1}{\overline{z} - \overline{z_i}}$$

where as usual the overbar denotes conjugation, and again we have taken all stars to be of one unit mass that determines our unit distance. The locations of the critical curves are found as usual by setting $\det A = 0$, which Witt shows is equivalent to

$$\frac{\partial w}{\partial \overline{z}} - \frac{\partial w}{\partial z} e^{i\phi} = 0$$

for some parameter $0 \leq \phi \leq 2\pi$ [15], [21]. This is then equivalent to a parametric representation of the critical curves

$$\gamma + \sum_{i=1}^{n} \frac{1}{(\overline{z} - \overline{z_i})^2} = e^{i\phi}.$$

For the simplest case of a single star located at the origin with no external shear ($\gamma = 0$, $n = 1$, $z_1 = 0$), the critical curve satisfies $\overline{z}^{-2} = e^{i\phi}$, producing two solutions $z = e^{-i\frac{\phi}{2}}$, $z = e^{-i(\frac{\phi}{2}+\pi)}$. These are easily recognizable as half circles in the complex plane, which together make the Einstein ring of the star.

Stepping back for a moment, in more physical terms, for our studies the critical curves are the locus of points where the total shear γ_{total} (which is a combination of the global external shear γ and that which is internally due to stars S) is equal to 1, as at those points $\mu^{-1} = 1 - \gamma_{total}^2 = 0$. When changing to complex variables, the shear can be written as $\gamma_{total} = \gamma_1 + i\gamma_2$, where the subscripts indicate the two independent components of the shear tensor.[1] By requiring $|\gamma_{total}|^2 = 1$ for the critical curves, we are left with a free parameter, which we designate as ϕ, which is the argument of the complex shear. Witt's parametric representation of the critical curves works then by providing all locations z whose total shear values lie on a unit circle in the complex plane.

[1] In terms of previous notation, $\gamma_1 = \gamma + S_1$ and $\gamma_2 = S_2$.

We define

$$F(\overline{z},\phi) = \gamma - e^{i\phi} + \sum_{i=1}^{n} \frac{1}{(\overline{z} - \overline{z_i})^2}$$

and note that $F(\overline{z},\phi) = 0$ is the parametric representation of the critical curves. As Witt points out, for any particular value of ϕ, F is of order $2n$ in $\overline{z}$. Thus we can discuss the problem of finding the values of z which are roots of F for a particular value of the parameter ϕ. Once these $2n$ roots have been found for a particular value (which we till take to be $\phi = 0$), we can vary ϕ by some small amount and iteratively create a list of solutions for various ϕ values, which can be mapped through the lens equation to determine their corresponding caustic locations. Visualizations of both can then be made, as well as calculations of values of interest like the caustic strength and total length of the caustics, as well as distributions and mean values of such.

We could use contour plots to simply capture where $F = 0$, much like we did to find the locations of micro-images. However, there are downsides to doing so. We will never be sure that all critical curves are found, as some could potentially escape any resolution we use in our plot. The locations found would give a value for $\overline{z}$, which we would then have to find the corresponding value of ϕ. In order to make sure all roots are found, we need values of $\overline{z}$ at the same ϕ value. We may as well make this our goal from the start and work towards accomplishing it.

Much like originally done for the the lens equation, roots of the parametric representation of the critical curves can be found by a grid search. This is a quick and efficient way to get a large number of roots (roughly n to $1.5n$), which makes finding the rest of the roots much easier. For low surface mass density and in the absence of external shear, we expect the critical curve of a single star to be the Einstein ring. In the presence of shear, they would be the "deltoids" or "astroids" of a Chang-Refsdal lens. From symmetry arguments regarding alignments with the external shear, we can expect solutions to be found near $\overline{z_i} \pm 1$ or $\overline{z_i} \pm i$, and so those are additional locations we perform initial root searches in.

Unlike the lens equation, the parametric representation of the critical curves is analytic in some variable (namely $\overline{z}$), and thus has a complex derivative. Taking an

initial value of $\phi = 0$, we now define

$$f(\overline{z}) = F(\overline{z}, 0) = \gamma - 1 + \sum_{i=1}^{n} \frac{1}{(\overline{z} - \overline{z_i})^2}$$

and

$$f'(\overline{z}) = \sum_{i=1}^{n} \frac{-2}{(\overline{z} - \overline{z_i})^3}.$$

We seek the $2n$ roots of $f(\overline{z})$. The argument principle of complex analysis tells us that

$$\frac{1}{2\pi i} \oint_C \frac{f'(\overline{z})}{f(\overline{z})} g(\overline{z}) d\overline{z} = \sum_a g(r_a) - \sum_a g(p_a)$$

for some region bounded by a curve C with winding number 0 for all $\overline{z}$ contained in C, and where r_a and p_a are the roots and poles of $f(\overline{z})$ respectively that lie within the region. We will take $g(\overline{z}) = (\overline{z})^N$, so that

$$\frac{1}{2\pi i} \oint_C \frac{f'(\overline{z})}{f(\overline{z})} (\overline{z})^N d\overline{z} = \sum_a r_a^N - \sum_a p_a^N.$$

By taking $N = 0$, we can find the number of roots of $f(\overline{z})$ contained in a region, minus the number of poles in that region. The only poles of $f(\overline{z})$ are the stars (each of which is of order two), thus we directly can find the number of roots. Upon comparison with the locations of the roots we have already found, we can determine whether a further search for roots has to be done in some region.

Thankfully, if there are unfound roots in a region we do not have to blindly search for them. Upon taking successive values of N and performing more integrations, we obtain algebraic equations for the roots which can be easily solved.

For example, if

$$\frac{1}{2\pi i} \oint_C \frac{f'(\overline{z})}{f(\overline{z})} d\overline{z} = 5$$

for some region with boundary C, and we find that 2 stars (each a double pole) lie within this region, we know that there must be 9 roots in the region. Suppose our grid

search has found 6 of them already, leaving 3 more to find. We can further evaluate

$$\frac{1}{2\pi i}\oint_C \frac{f'(\overline{z})}{f(\overline{z})}(\overline{z})^N d\overline{z}$$

for $N = 1, 2, 3$, thus obtaining a set of equations

$$r_1 + r_2 + r_3 = \frac{1}{2\pi i}\oint_C \frac{f'(\overline{z})}{f(\overline{z})}(\overline{z})d\overline{z} + 2\sum_{a=1}^{2} s_a - \sum_{f=1}^{6} r_f \equiv c_1$$

$$r_1^2 + r_2^2 + r_3^2 = \frac{1}{2\pi i}\oint_C \frac{f'(\overline{z})}{f(\overline{z})}(\overline{z})^2 d\overline{z} + 2\sum_{a=1}^{2} s_a^2 - \sum_{f=1}^{6} r_f^2 \equiv c_2$$

$$r_1^3 + r_2^3 + r_3^3 = \frac{1}{2\pi i}\oint_C \frac{f'(\overline{z})}{f(\overline{z})}(\overline{z})^3 d\overline{z} + 2\sum_{a=1}^{2} s_a^3 - \sum_{f=1}^{6} r_f^3 \equiv c_3$$

where we have brought together on the right hand side the integral and our known information (the 2 stars s_a, each of which contributes twice since they are double poles, and the 6 already found roots r_f).

5.3 Simulations for the parameters of Huchra's lens

We perform calculations for the parameters used in our study of the macro-saddles of Huchra's lens, namely $\kappa = 0.73$, $\gamma = 0.72$ and $\kappa = 0.62 = \gamma$. We use fields of 500 stars, and tesselate our field into square regions to make the integrations around C simple. We take $\Delta\phi = \frac{2\pi}{200}$ after our initial points are found. We note that we could have used the star fields provided by Dr. Wambsganss, but our code was not quite optimized enough yet to get results in a timely manner. Compared with Witt 1990, where calculations took one hour for similar parameters as ours, our calculations took approximately 10 minutes (so not quite as fast as they could be. We expect that we will be able to speed up the process in future work). Preliminary critical curves and caustics are shown in 5-1, with a closer view of the caustics shown in 5-2.

Far away from the center of the field of stars, the critical curve and caustic take on the shape of that for a Chang-Refsdal lens, albeit one with 1000 times the mass used

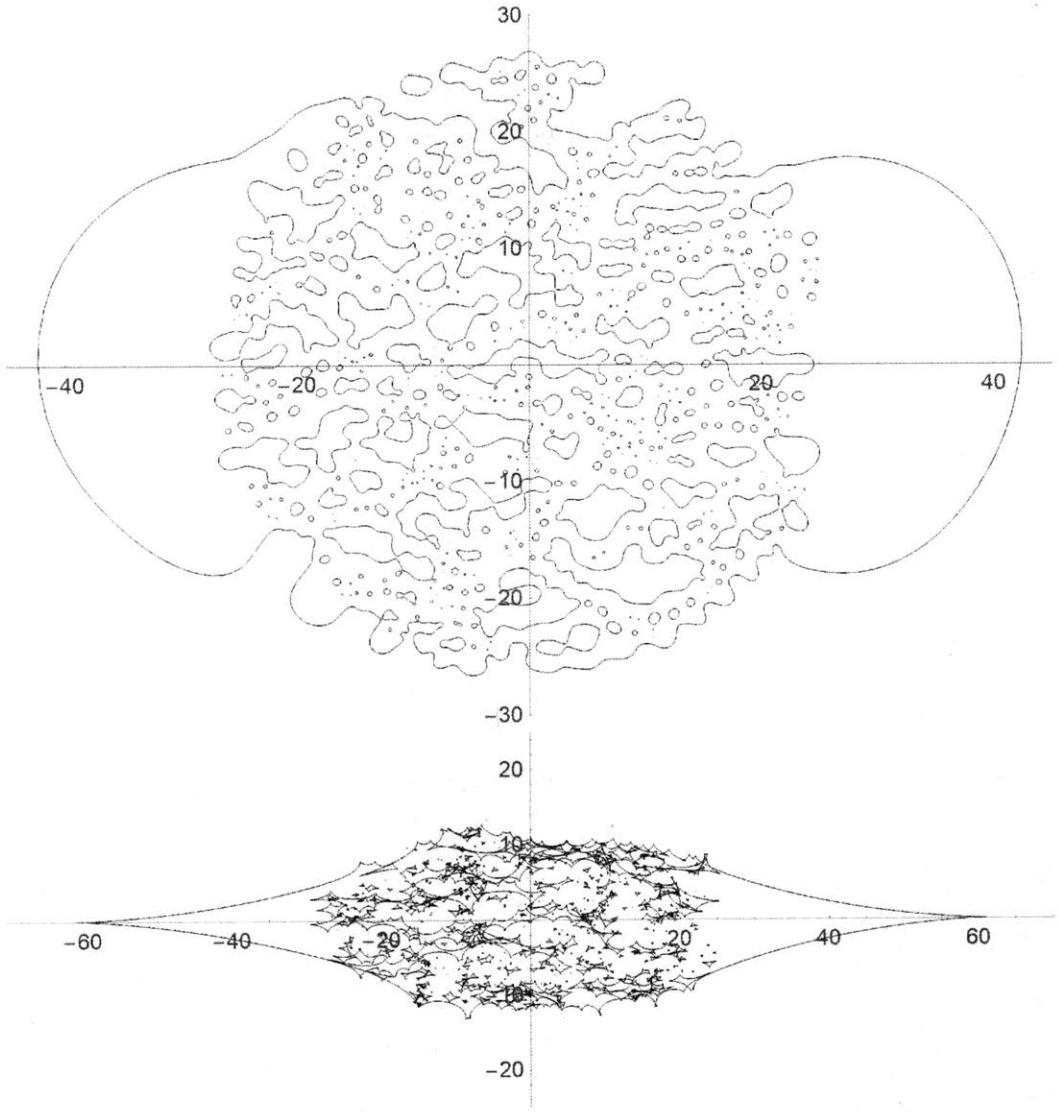

Figure 5-1: Critical curves and caustics for $\kappa = 0.73$, $\gamma = 0.72$
Critical curves and caustics for κ and γ corresponding to one of the macro-saddles of Huchra's Lens. Far away from the center of the field of stars, the critical curve and caustic take on the shape of a single lens, with mass equal to 1000 of our unit mass, embedded in an external shear field (Chang-Refsdal lens).

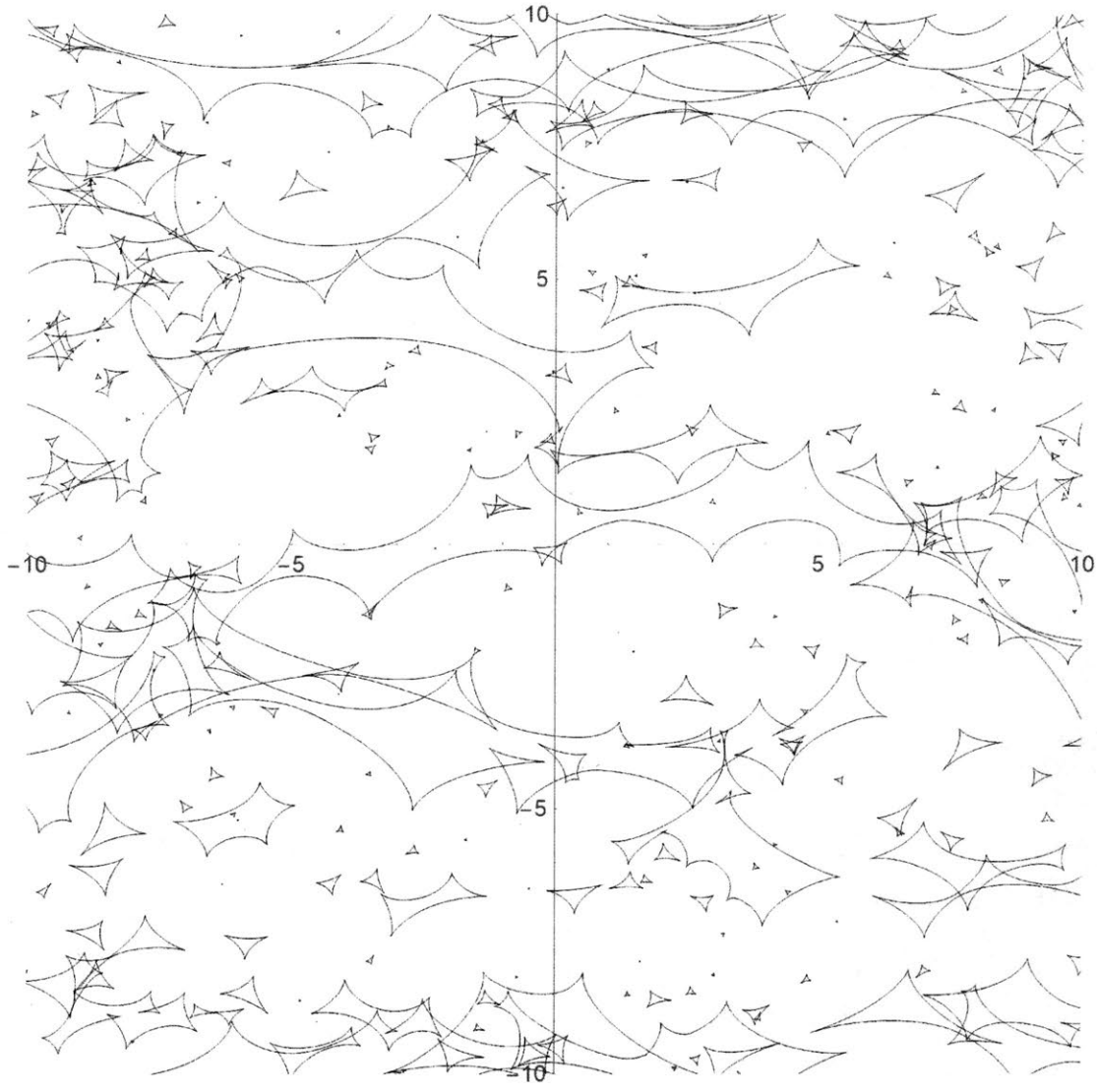

Figure 5-2: Zoom of the caustics for $\kappa = 0.73$, $\gamma = 0.72$
Zoom of the caustics for figure 5-1.

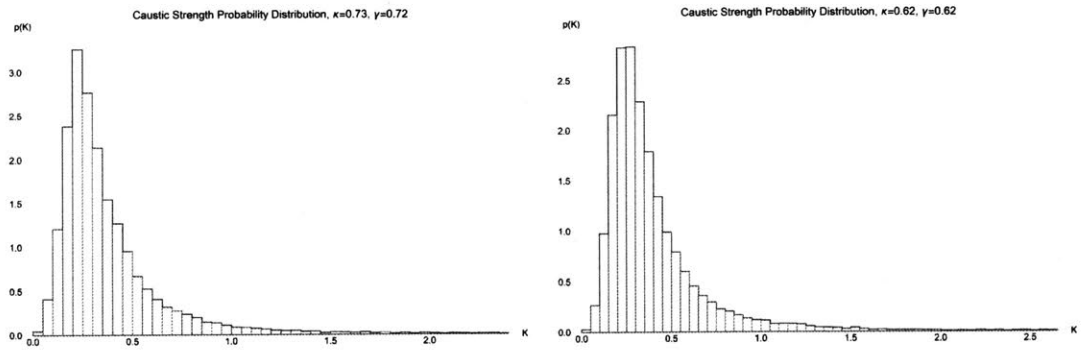

Figure 5-3: Probability distributions of the caustic strength for macro-saddles of Huchra's lens
Probability distribution of the caustic strength for $\kappa = 0.73$, $\gamma = 0.72$ (left) and $\kappa = 0.62 = \gamma$ (right). Bins are of size 0.05, and we show $\langle K \rangle \pm 3\sigma_K$.

for the individual stars. These edge affects are consequences of a finite field of stars. As Witt does, for further calculations we select those critical curves which lie within a radius 0.9 times that used to create the star field, and likewise only the caustics which they map to.

Knowledge of the locations of the critical curves and caustics allows us, as Witt did, to find mean values for the strength of the caustic $\langle K \rangle$, the square of the strength $\langle K^2 \rangle$, and the caustic length produced by a single star $\langle \lambda_\star \rangle$.

We calculate the value of K at every critical curve position found. While these positions are equally spaced over ϕ, they are not necessarily evenly spaced in the plane of the caustic. We assume that K varies smoothly and is approximately constant over some small caustic length $d\lambda$. For a particular caustic point, we calculate the sum of half the distance to the preceding point and half the distance to the succeeding point. We then divide by the total length of the caustic to get a probability with which to weight the caustic strength K at that point.

We find for $\kappa = 0.73$, $\gamma = 0.72$ that the total length of the caustics is 1217.216. This corresponds to a value of $\langle \lambda_\star \rangle = 3.005$. We also find $\langle K \rangle = 0.417$, $\langle K^2 \rangle = 0.597$, and $\sigma_K = \sqrt{\langle K^2 \rangle - \langle K \rangle^2} = 0.651$.

We find for $\kappa = 0.62 = \gamma$ that the total length of the caustics is 1419.476, corresponding to $\langle \lambda_\star \rangle = 3.505$. We find $\langle K \rangle = 0.445$, $\langle K^2 \rangle = 0.729$, and $\sigma_K =$

$\sqrt{\langle K^2 \rangle - \langle K \rangle^2} = 0.729$.

The probability distributions $p(K)$ can be seen in figure 5-3 for the two cases. The values for $\langle K \rangle$ are in agreement with the values we found in Chapter 3 for a small sampling of points, though our values for σ_K are much different. We suspect this is due to somehow not fairly sampling the caustic network with the two source tracks we took.

Chapter 6

Animations of Microlensing

6.1 What does animation add

The individual images produced by micro-lensing are unresolvable in the sky. The magnification maps and caustic networks commonly used to statistically study micro-lensing events only show what the combined light from the micro-images actually does as the source moves. A visualization of the behavior of the micro-images for pedagogical purposes was made in the form of a video. That video cannot be included in its entirety here on paper, but a brief explanation of it can be.

6.2 Creating the video

Given the star positions that create the caustic networks in Dr. Wamsbganss' magnification maps, I was able to find the locations of every micro-image for a given source position. Once known, the magnifications of the micro-images could be determined as well. A plot of the positions of the stars along with the positions of the micro-images could then be created, as was shown in figure 3-3.

In order to more aesthetically show what is happening, some modifications were made to the output in 3-3. The background was changed to black, with white stars as circles.

Our source is an ideal point source. However, it is known that a circular source

produces (to first order) elliptical images in the image plane, whose area, semi-major axes, and orientation depend on the magnification and shear that the image experiences at its location. Therefore, I let the micro-images be ellipses that show up among the stars. The sizes of the ellipses scale logarithmically with their magnifications, in order to have a dynamic range that doesn't overwhelm at regions near caustics yet still allows for the viewing of images with low magnifications. In particular, the scaling goes as $A(\mu) = \ln(a \cdot \mu + b)$, where $A(0) = 0$ and $A(1) = 1$. The micro-minima are then represented in blue and micro-saddles in orange. The profiles for both the stars and the micro-images are Gaussian. In regions where the images which are micro-minima and micro-saddles overlap, the blue and orange are added together to produce white, demonstrating the flash of light and increase in magnification that comes from the creation or annihilation of a pair of micro-images. An example frame is shown in figure 6-1.

The figure created is a single snapshot, but given a track for the source through the caustic network multiple snapshots can be made and strung together to see how the micro-images move, are created, and are annihilated as the source changes position. A sequence of snapshots is shown in figure 6-2, demonstrating the source position at three different points and the behavior of the micro-images.

The video combines the snapshots of images and the caustic network by displaying the movement of the source among the caustics on one side and the movement of images on the other. Thus, by watching the position of the source on the left one can anticipate the creation or annihilation of images on the right. A bar along the top of the screen can show the lightcurve of the source as it moves, as well as the number of micro-minima as a function of source position.

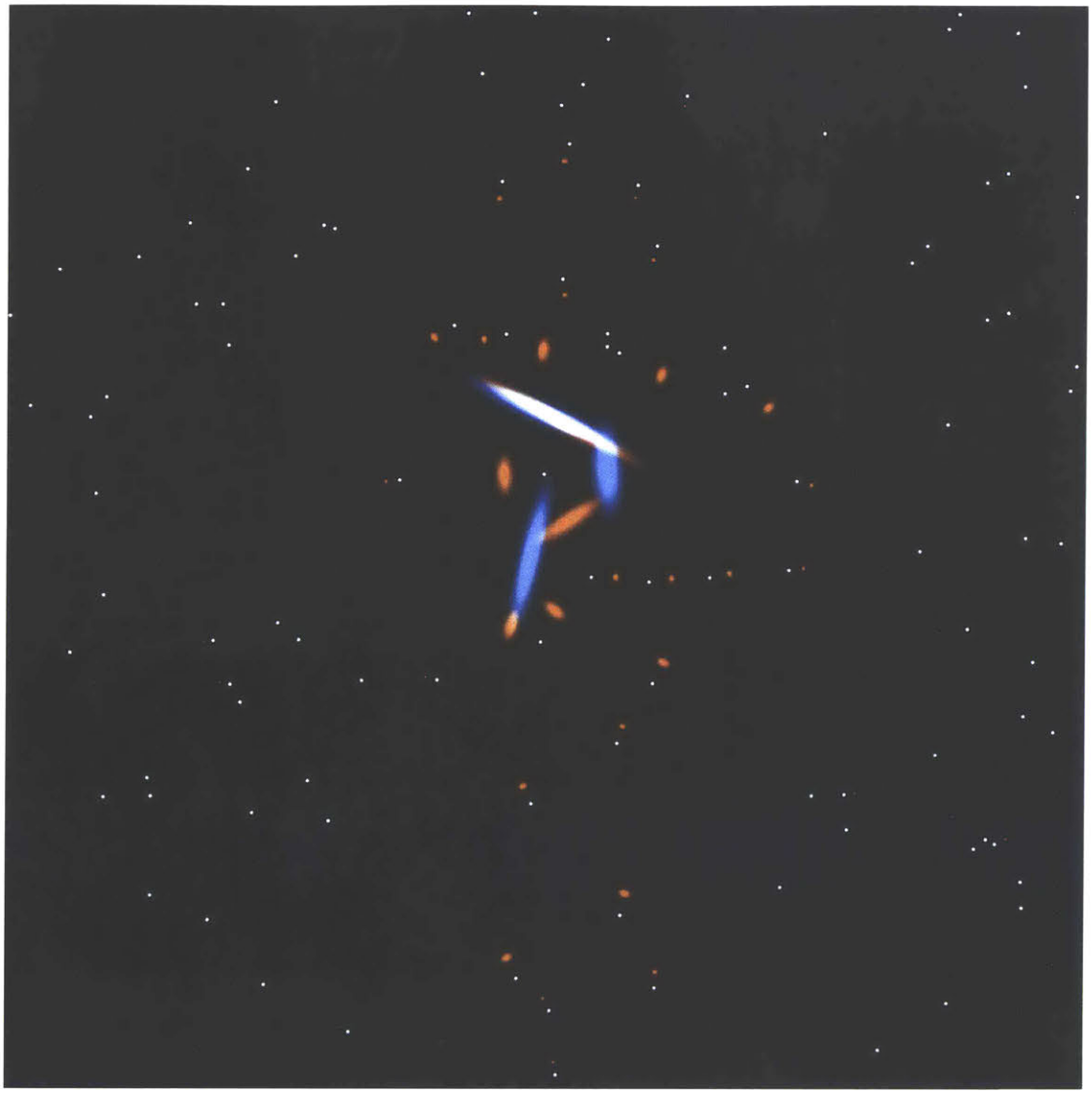

Figure 6-1: Sample frame from the video
Sample frame for the same configuration that produced figure 3-3, though zoomed in at the center to a quarter of the area. The sizes of the images are exaggerated, as an ideal point source would technically produce point images. However, a small circular source would produce elliptical images to first order, and we have chosen to scale the size of the images logarithmically with their magnification. Note how the bright, visible images in general extend along the vertical direction (the direction the global shear would stretch an image in the absence of stars).

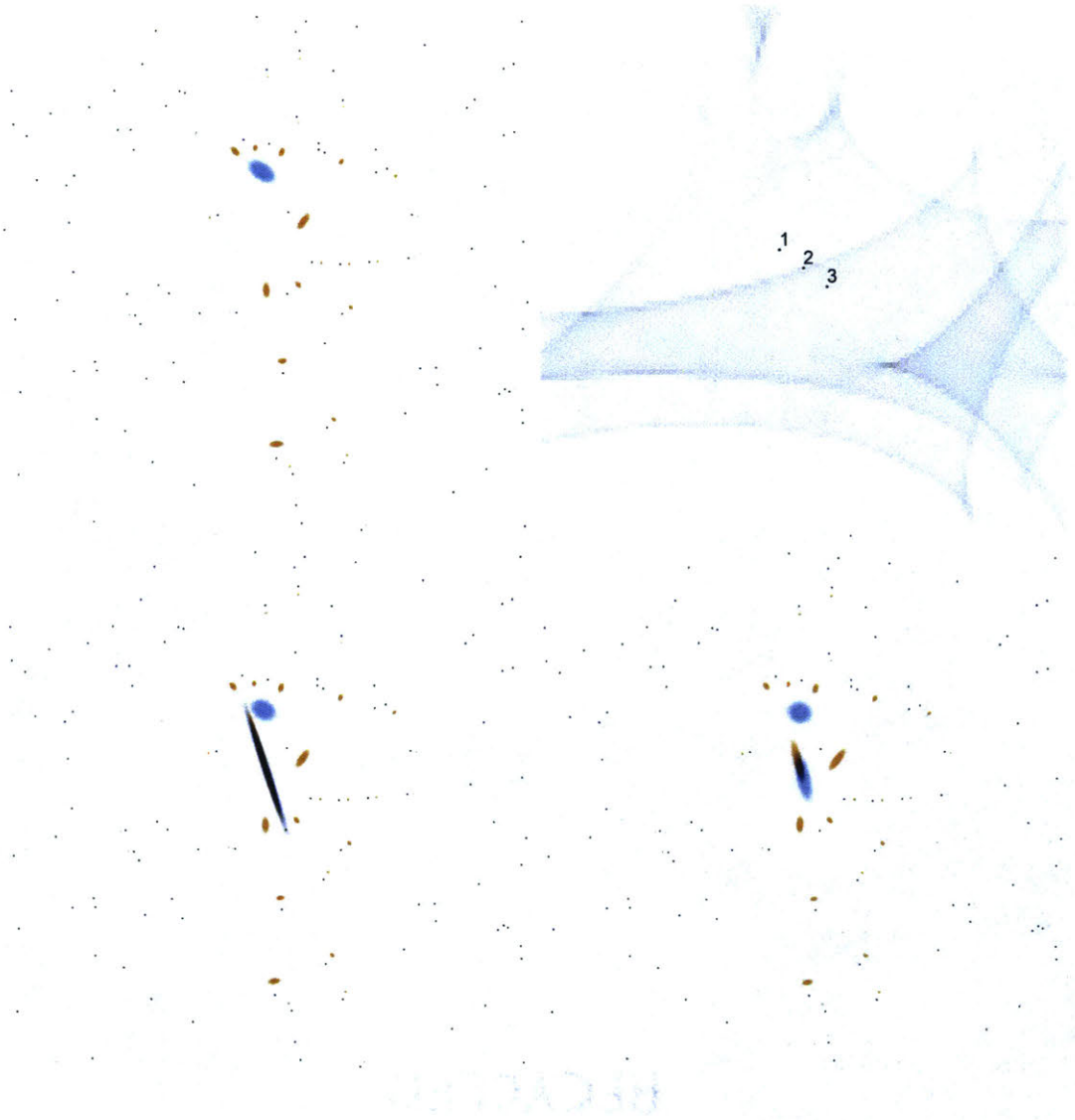

Figure 6-2: Set of inverted color frames from the video
Counter clockwise from top right: 3 source positions within the caustic network, micro-images corresponding to position 1, micro-images corresponding to position 2, micro-images corresponding to position 3. The source moves between two regions with varying numbers of micro-images, and the three frames show the micro-images for each of the two regions as well as for a position close to the caustic separating them. The frames are (almost) inverted in color from the actual movie. We keep our convention that micro-minima are blue and micro-saddles are orange, thus simply reversing the color of the background and stars. A new pair of images emerges at position 2. Note how the shear affecting the only micro-minimum present in the upper left varies as the source moves, changing the micro-image from an elliptical to a more circular shape.

Chapter 7

Lensing Near Macro-Caustics

7.1 Motivation

While the individual stars in a galaxy create their own micro-critical curves which map to micro-caustics, the smoothed out matter distribution of a galaxy or a cluster of galaxies produces a macro-critical curve and a macro-caustic as well. A source crossing a macro-caustic causes the creation or annihilation of a pair of macro-images. But as we know, these macro-images are actually composed of thousands of micro-images.

Prompted by new observations, recent papers have only just begun to examine some of the properties of micro-lensing near macro-caustics [18]. There is a rich realm to be explored yet, and we hope to start scratching the surface here.

7.2 Preliminary information

A macro-caustic can be caused by a gradient in the external shear, which we have taken to be a constant at the location of a macro-image up to this point. Again starting by ignoring the presence of micro-lenses, a Taylor expansion of the time delay near the vicinity of a fold macro-caustic gives a lens equation of the form

$$y_1 = \tau_{11} \cdot x_1$$
$$y_2 = \frac{1}{2}\tau_{222} \cdot x_2^2$$

in a coordinate system such that $\tau_{12} = \tau_{22} = 0$ (where subscripts denote derivatives with respect to x_1 or x_2, and the derivatives are evaluated at our expansion point) [2], [15], [20]. Our macro-critical curve is then the x_1 axis, and our macro-caustic is the y_1 axis.

We again take $\kappa \equiv \kappa_{dark} = 0$ initially, and note that $\tau_{11} + \tau_{22}$ (the trace of the magnification matrix) is always equal to $2 - 2\kappa$. We rewrite τ_{222} in terms of the single macro-image strength of our caustic, $K = \sqrt{\frac{1}{2(\tau_{11})^2 \tau_{222}}}$, to arrive at

$$y_1 = 2x_1$$
$$y_2 = \frac{1}{2} \cdot \frac{1}{8K^2} \cdot x_2^2$$

Note that K^2 has units of distance, the scale for which we specify later. Micro-lenses with some $\kappa_\star$ are then added, while simultaneously subtracting an equivalent κ_{dark} (such that our initial κ=0 does not change) from the smooth potential. Since we initially chose $\kappa_{dark} = 0$, this has the effect of introducing a negative smooth surface mass density. Gravity has no objections to negative mass, though it may not happen to exist. This produces

$$\vec{y} = \begin{pmatrix} (2 + \kappa_\star)x_1 & 0 \\ 0 & \frac{1}{16K^2}x_2^2 + \kappa_\star \cdot x_2 \end{pmatrix} - \theta_E^2 \sum_i^n \frac{m_i \cdot (\vec{x} - \vec{x_i})}{|\vec{x} - \vec{x_i}|^2}$$

With minor modifications to code, we are able to examine the behavior of micro-images moving around as the source passes through the micro-caustic network of a macro-caustic.

7.3 Simulations

We spread 1000 stars of equal mass (which again sets our unit distance scale θ_E) in a circle of radius R such that $\kappa_\star = 0.01$ (an approximate value for the intra-cluster medium where the macro-caustics of galaxy clusters occur). We rewrite our lens equation slightly again by noting the following: while $\mu \approx \frac{K}{\sqrt{d}}$ in terms of distance from the caustic (where $d = y_2$ is perpendicular to the caustic in our coordinate system), we can use $y_2 = \frac{1}{2} \cdot \frac{1}{8K^2} \cdot x_2^2$ to rewrite this as $\mu \approx \frac{4K^2}{x_2}$ where x_2 is perpendicular to the critical curve. We justify using this approximation (which we have shown to be incorrect on a micro-caustic scale!) momentarily. We can then designate some distance L in the image plane and the magnification μ_L associated with that distance to determine K, giving

$$\vec{y} = \begin{pmatrix} (2+\kappa_\star)x_1 & 0 \\ 0 & \frac{1}{4 \cdot L \cdot \mu_L} x_2^2 + \kappa_\star \cdot x_2 \end{pmatrix} - \theta_E^2 \sum_i^n \frac{m_i \cdot (\vec{x} - \vec{x_i})}{|\vec{x} - \vec{x_i}|^2}.$$

We take $\mu_L = 30$ at a distance $L = R/\sqrt{2}$, thus stipulating that our star field only covers a region of length ≈ 0.001 in units of the caustic strength and (hopefully) avoiding any possible side-affects of the approximation for the magnification. In units of the Einstein radius of the stars then, this means that we have $K^2 \approx 1677$. These parameters produce the critical curves shown in 7-1.

The magnification matrix at a point is given by

$$A = \begin{pmatrix} (2+\kappa_\star) + S_1 & S_2 \\ S_2 & \frac{1}{2 \cdot L \cdot \mu_L} x_2 + \kappa_\star - S_1 \end{pmatrix}.$$

Given how we selected L, along with our value for $\kappa_\star$, if the shear from the stars is not substantial (i.e. our micro-images are far away from the stars, which is more likely than not with a low surface mass density) then the inverse magnification matrix

$$A \approx \begin{pmatrix} 2 & 0 \\ 0 & 0 \end{pmatrix}.$$

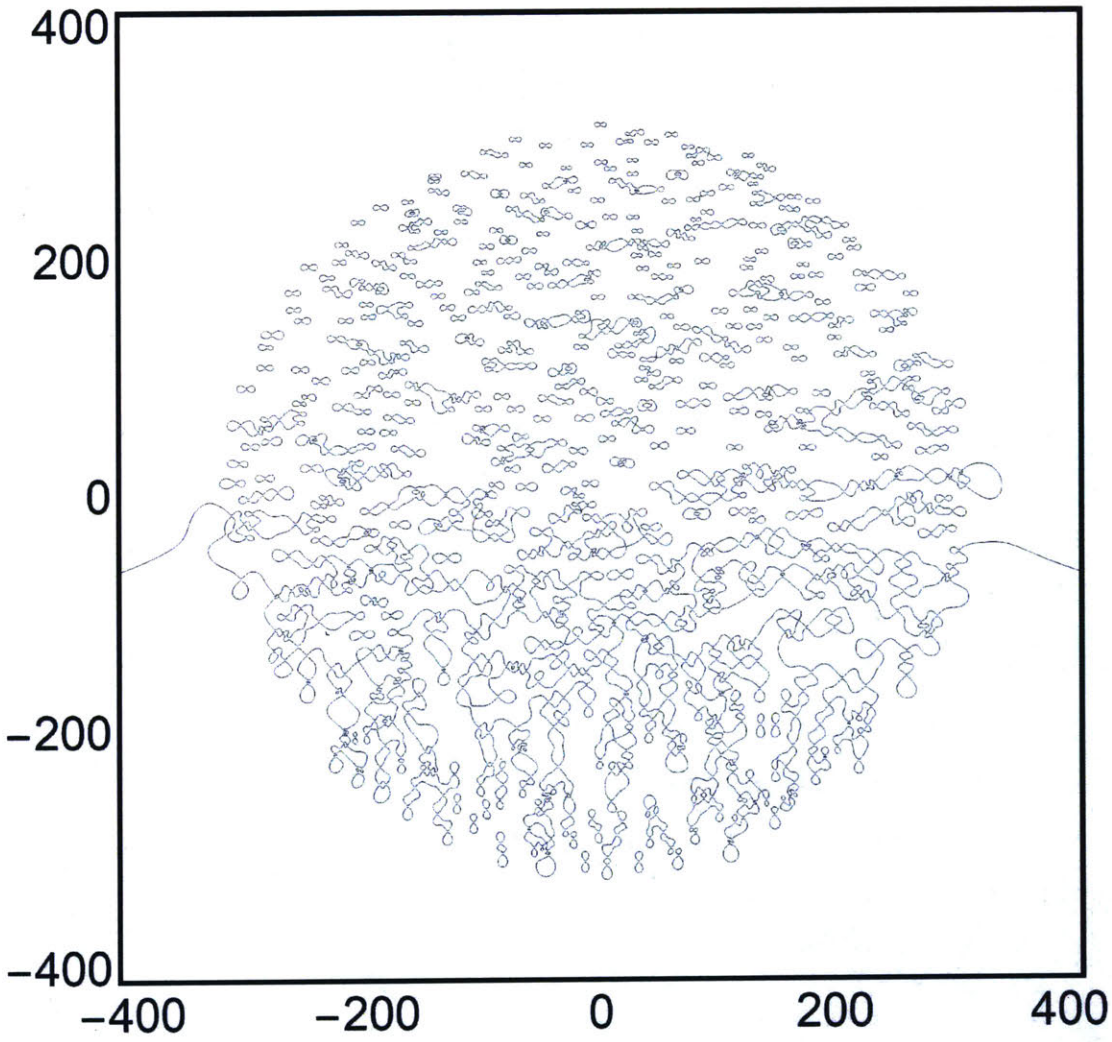

Figure 7-1: Critical curves for micro-lenses perturbing a macro-critical curve
The micro-critical curves produced by a field of stars perturbing a smooth macro-critical curve. Units are in terms of the Einstein ring of a single star. Note that outside the field of stars, the complicated twists of the micro-critical curves rejoin the smooth macro-critical curve. This smooth macro-critical curve is offset from our desired macro-critical curve of the x_1 axis inside the field of stars, due to our subtraction of $\kappa_\star$ from the smooth potential. Compare "smooth critical curve" vs. "macro-critical curve" in 2.2 of [18], as well as fig. 4 of [18].

This is somewhat redundant, given that we set up our system around a macro-critical curve. But there are a couple things worth pointing out. On a large scale, a change in distance in the image plane Δx_2 becomes a highly suppressed Δy_2, whereas any Δy_1 is approximately equal to $2\Delta x_1$.

This is apparent in examining the caustic network, as seen in figure 7-2. Note the extreme scaling differences in the two directions.

To first order, macro-images of a circular source would be ellipses, with semi-major axes determined by the magnification matrix. Thus a circular source of radius r produces elliptical images with semi-major axes $r_{x_1} \approx r/2$ and $r_{x_2} \approx \infty$. We expect the micro-images of the source to produce a highly elongated train extending along the x_2 direction. This is beneficial: it reduces the problem to a (nearly) one dimensional examination of how micro-images behave.

We can again search for the micro-images created by a given source position in the caustic network. The results for various source positions are shown in figure 7-3, with a zoom in 7-4. The motion of the train of images comprising the macro-saddle and the macro-minimum towards each other is easily seen. They begin to merge together somewhere around when the source crosses $y_2 \approx 0.5$, converging and finally completely annihilating at a point slightly off of the macro-critical curve after the source crosses $y_2 \approx -0.5$. New micro-images seem to always appear between the trailing bright images of each train. This has the effect that micro-minima always move towards decreasing x_2, whereas micro-saddles always move towards increasing x_2, the same as the macro-images. A created pair of images can strictly never annihilate themselves together then if this is the case.

While many more simulations would need to be done to gain a better empirical idea of how the micro-images behave, this single examination has provided a starting point for future work that we hope to expand upon.

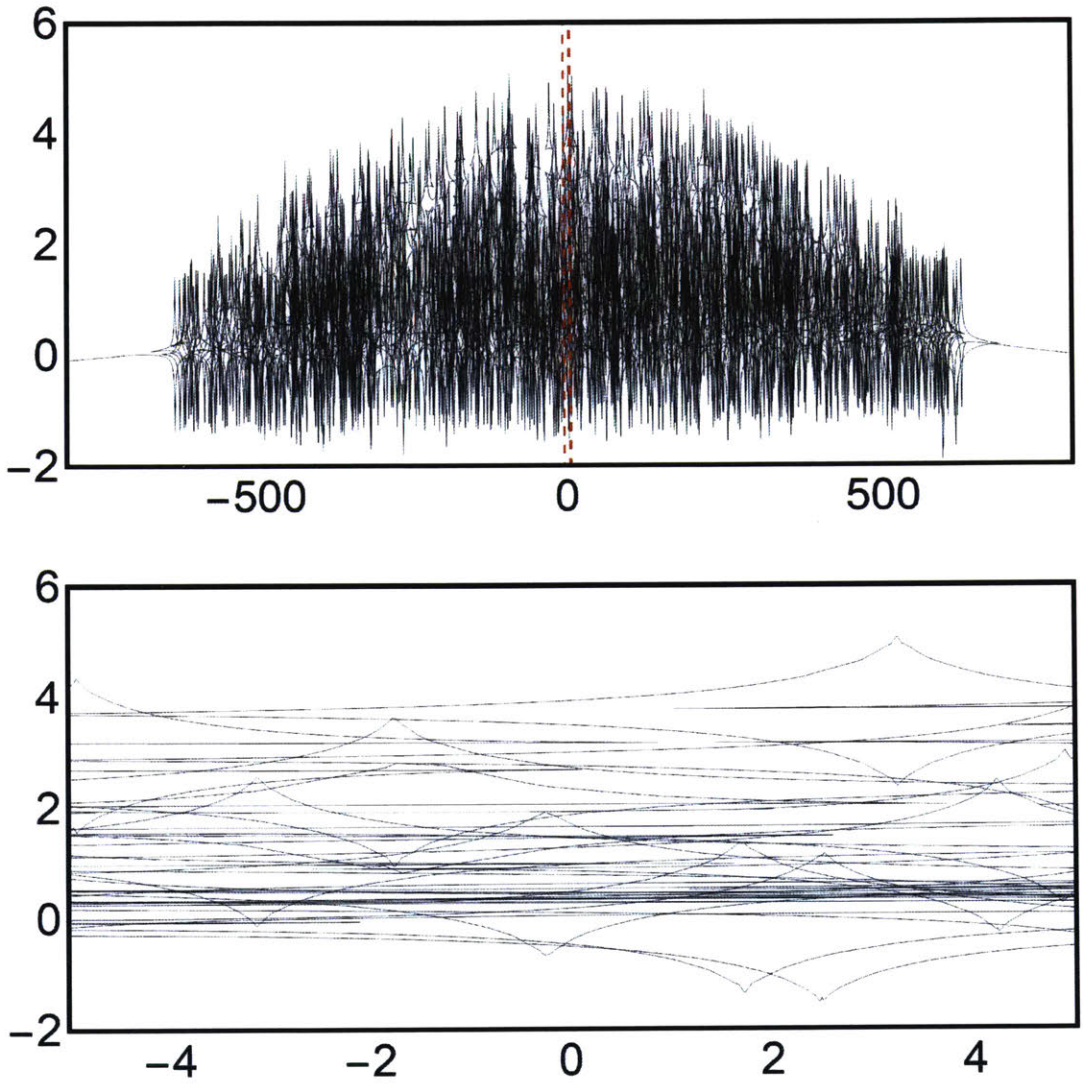

Figure 7-2: Micro-caustic network for a macro-caustic
Top: the micro-caustic network for the critical curves of figure 7-1. Bottom: zoom in of the red boxed region of the top. Units are in terms of the Einstein ring of a single star. Note the vast difference in scale of the top figure, demonstrating how changes in distance perpendicular to the critical curve correspond to highly suppressed distances perpendicular to the caustic. The caustics of the stars are approximately those of Chang-Refsdal lenses. In the bottom, we see that the caustics are highly stretched perpendicular to the caustic, making it likely that a source moving through the network passes through the cusps of many caustics. Compare figure 5 of [18].

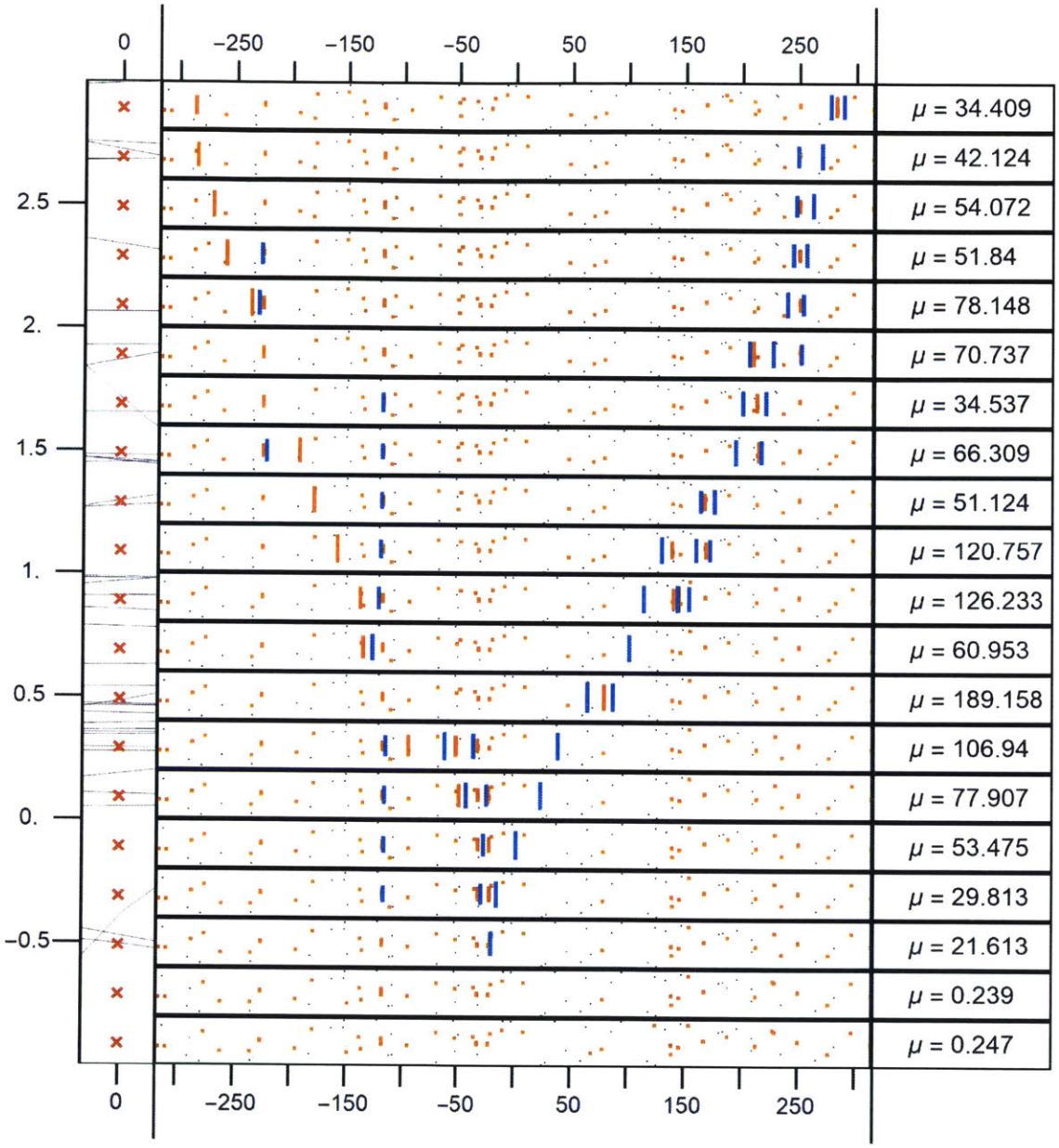

Figure 7-3: Micro-image positions for a source moving through a caustic network Left: further zoom of the micro-caustic network for a macro-caustic as shown in figure 7-2. The red markers represent the positions of the source. The source is moving perpendicular to the caustic along y_2, with $y_1 = 0$. Middle: the micro-images that appear due to the source positions on the left. We have rotated our coordinate system to take advantage of the one-dimensional nature of the locations of the images. The positive x_1 directon points down, and the positive x_2 direction points to the right. Each strip is centered on $(0, 0)$. We have adapted a combination of plotting methods shown previously. Minima are presented as blue, and saddles as orange, lines. The lengths of the line scaless logarithmically with their magnification. Right: the total magnification of each strip.

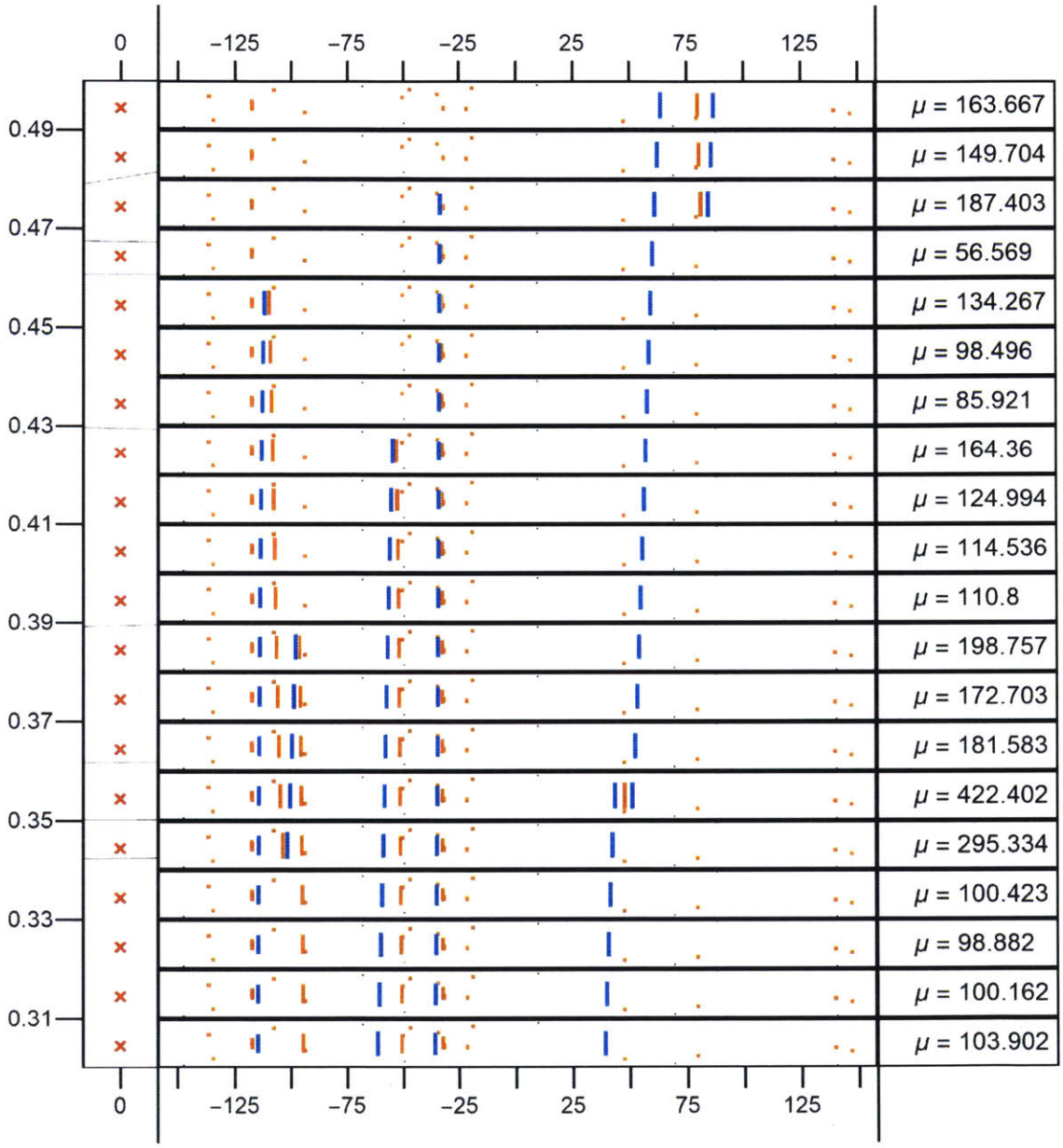

Figure 7-4: Yet more micro-image positions for a source moving through a caustic network

Left: yet a further zoom of the micro-caustic network. Middle: the micro-images that appear due to the source positions on the left. We have selected a portion of the caustic network with the most action. Right: total magnification of each strip.

Chapter 8

Closing Remarks

We set out to examine the behavior of micro-images near caustic crossing events, and have showed that at high optical depth an approximation used for the temporal variations in flux breaks down at a strength-scaled distance from the caustic of $\approx$ 0.1. Modifications to the approximation, which can potentially draw from statistics involving the mean micro-minima magnifications, may provide a somewhat better analysis for such events. Lensing near macro-caustics disturbed by the micro-caustics of stars opens a further field to be explored with our methods as well.

As mentioned by Wambsganns, Witt, and Schneider [19], a full analysis of micro-lensing can benefit greatly from the three combined methods of ray-tracing, image positin determination, and knowledge of the caustic network location. We are approaching a point where this is feasible, and look forward to seeing what future work may hold in store.

Bibliography

[1] Jin H. An and N. Wyn Evans. The chang-refsdal lens revisited. *Monthly Notices of the Royal Astronomical Society*, 369(1):317–334, 2006.

[2] Roger Blandford and Ramesh Narayan. Fermat's principle, caustics, and the classification of gravitational lens images. *The Astrophysical Journal*, 310:568–582, 15 November 1986.

[3] K. Chang and S. Refsdal. Flux variations of qso 0957+561a,b and image splitting by stars near the light path. *Nature*, 282:561–564, 6 December 1979.

[4] K. Chang and S. Refsdal. Star disturbances in gravitational lens galaxies. *Astronomy and Astrophysics*, 132(1):168–178, March 1994.

[5] Johnathan Granot, Paul L. Schechter, and Joachim Wambsganss. The mean number of extra microimage pairs for macrolensed quasars. *The Astrophysical Journal*, 583(2):575–583, 20 December 2003.

[6] Neal Katz, Steven Balbus, and Bohdan Paczynski. Random scattering approach to gravitational microlensing. *The Astrophysical Journal*, 306:2–8, 1 July 1986.

[7] R. Kayser and H. J. Witt. Amplification near gravitational lens caustics. *Astronomy and Astrophysics*, 221(1):1–3, August 1989.

[8] Geraint F. Lewis, Jordi Miralda-Escude, Derek C. Richardson, and Joachim Wambsganss. Microlensing light curves: a new and efficient numerical method. *Monthly Notices of the Royal Astronomical Society*, 261(3):647–656, April 1993.

[9] E. Mediavilla, J. A. Muoz, P. Lopez, T. Mediavilla, C. Abajas, C. Gonzalez-Morcillo, and R. Gil-Merino. A fast and very accurate approach to the computation of microlensing magnification patterns based on inverse polygon mapping. *The Astrophysical Journal*, 653(2):942–953, 1 February 2006.

[10] Ramesh Narayan and Matthias Bartelmann. Lectures on gravitatational lensing. 1995.

[11] Rajaram Nityananda and J. P. Ostriker. Gravitational lensing by stars in a galaxy halo: theory of combined and strong scattering. *Journal of Astrophysics and Astronomy*, 5:235–250, September 1984.

[12] Bohdan Paczynski. Gravitational microlensing at large optical depth. *The Astrophysical Journal*, 301:503–516, 15 February 1986.

[13] A. O. Petters, H. Levine, and J. Wambsganss. *Singularity Theory and Gravitational Lensing*. Springer, 2001.

[14] Paul L. Schechter and Joachim Wambsganss. Quasar microlensing at high magnification and the role of dark matter: enhanced fluctuations and suppressed saddle points. *The Astrophysical Journal*, 580:685–695, 1 December 2002.

[15] P. Schneider, J. Ehlers, and E. E. Falco. *Gravitational Lenses*. Springer, 1999.

[16] P. Schneider and Weiss. A gravitational lens origin for agn-variability? consequences of micro-lensing. *Astronomy and Astrophysics*, 171:49–65, 1987.

[17] V. N. Shalyapin, L. J. Goicoechea, D. Alcalde, E. Mediavilla, J. A. Munoz, and R. Gil-Merino. The nature and size of the optical continuum source in qso 2237+0305. *The Astrophysical Journal*, 579:127–135, 1 November 2002.

[18] Tejaswi Venumadhav, Liang Dai, and Jordi Miralda-Escude. Microlensing of extremely magnified stars near caustics of galaxy clusters. *The Astrophysical Journal*, 850(1):49, 20 November 2017.

[19] J. Wambsganss, H. J. Witt, and P. Schneider. Gravitational microlensing: powerful combination of ray-shooting and parametric representation of the caustics. *Astronomy and Astrophysics*, 258(2):591–599, May 1992.

[20] Joachim Wambsganss. PhD thesis, Thesis Ludwig-Maximilians-Univ., Munich (Germany, F. R.). Fakultät für Physik, January 1990.

[21] H. J. Witt. Investigation of high amplification events in light curves of gravitationally lensed quasars. *Astronomy and Astrophysics*, 236:311–322, 1990.

[22] H. J. Witt. An efficient method to compute microlensed light curves for point sources. *The Astrophysical Journal*, 403:530–541, 1993.